FreshAir Sensor LLC
16 Cavendish Ct
Lebanon, NH 03766
info@freshairsensor.com

Re: FreshAir Sensor Reports as Proof of Smoking Events

To whom it may concern,

FreshAir Sensor's patented sensors are the only technology available that can monitor for and specifically detect tobacco smoke and marijuana smoke. FreshAir has 5 patents issued and many more pending.

FreshAir is widely deployed in hotels, apartments, and schools.

FreshAir's sensors detect specific molecular components of tobacco smoke and marijuana smoke. FreshAir doesn't send alerts based on candles, incense, dust, steam, or other non-smoking sources. A smoking alert from FreshAir scientifically proves that smoking took place in a monitored space.

This page is followed by a series of documents which demonstrate FreshAir Sensor's deep scientific background and demonstrated performance.

There is a detailed description of how the technology works, which includes the professional background of FreshAir's inventor. There is an excerpt from a court case where FreshAir's sensors were specifically accepted as evidence. Finally there are three peer reviewed scientific articles which describe FreshAir's sensor technology.

If you have any questions on this technology please contact FreshAir at info@freshairsensor.com or call 603.643.7181.

Sincerely,

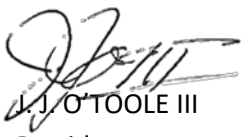

J. J. O'TOOLE III
President

Joseph J. BelBruno, Ph.D.
FreshAir Sensor, LLC
16 Cavendish Court
Lebanon, NH 03766
info@freshairsensor.com
+1-603-643-7181

Brief description of FreshAir Sensor technology to detect tobacco and marijuana smoke

FreshAir Sensor's devices detect specific molecular components of tobacco smoke and marijuana smoke with patented, polymer sensor technology (PolySens®). The devices have Wi-Fi capabilities for real-time monitoring, enabling FreshAir's clients to monitor and deter smoking in prohibited areas. FreshAir's devices are unique and not what one considers "typical" smoke detectors, such as those used in apartments, homes and hotels for fire protection. Typical smoke detectors are indiscriminately triggered by any obstruction of the beam path within the device, as shown below. That obstruction may be caused by a significant number of any particles (dust, pollen, smoke, steam or other). For example, fire protection smoke detectors are triggered by steam and smoke from cooking, but FreshAir sensors are not. FreshAir sensors are triggered by the presence of marijuana or tobacco smoke, while fire protection sensors typically are not. FreshAir's sensors detect and allow property managers to reduce or eliminate the presence of secondhand smoke, the smoke to which non-users of marijuana and tobacco are subjected when others smoke nearby.

Operation of a Typical Smoke Detector

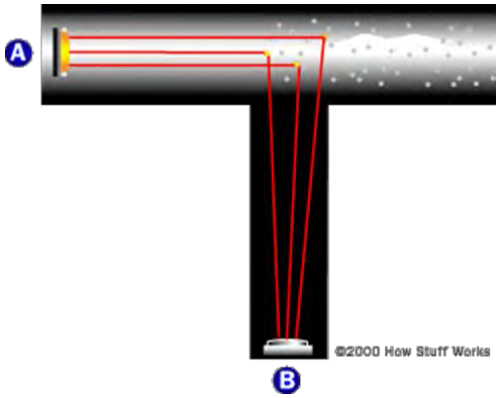

If sufficient particles enter a typical smoke detector, light from the source (A) is reflected toward the photocell (B), and the alarm is sounded. A large number of particles is required to trigger the alarm, and there is no way to determine the type of particles present.

FreshAir's device, which plugs into a standard wall outlet, *is triggered only by smoke that results from burning tobacco or marijuana in the protected space*. The sensor within the device contains receptors that are sensitive only to specific molecular components of such smoke. Unlike a typical smoke detector, it will not be triggered by other combusting materials, such as paper, food or incense, nor will it be triggered by dust or steam. Once triggered, the FreshAir device automatically sends an alert to FreshAir's server. That alert includes the device's unique identifier and data collected immediately before and during the event. FreshAir then notifies the property manager of the event by sending an electronic message that identifies the specific device and includes a time-stamped graph that shows the buildup and decay of the sensor output that corresponds to the smoking violation. The process is shown schematically below.

The sensor within FreshAir's device is based on polymer thin film technology. The film contains specific binding sites which bind only the target molecule; the binding sites do not bind other molecules. When the target molecule is bound to the polymer film, the electrical properties of the film change in proportion to the amount of the target molecule present. The changes in the electrical properties of the sensor as the target molecule is bound are positive evidence of the presence of either tobacco or marijuana smoke, as appropriate.

Operation of FreshAir's Device:

The presence of only tobacco or marijuana smoke triggers the sensing device that alerts FreshAir of the incident. FreshAir's cloud-based monitoring platform then passes on the time-stamped alert of the incident to the property manager's representative.

Basic FreshAir Sensor Functionality:

A polymer film in the FreshAir device contains binding sites that are chemically and spatially designed to bind the target molecule (in the current case, specific molecules that are unique components of tobacco and marijuana smoke). The sensor does not respond to other sources of smoke. When confronted with a mixed sample of gases (top figure below), only the target molecule effectively binds to the film. Presence of the target molecule changes the electrical properties (resistance) of the film. The electrical properties of the film are measured by a set of electrodes. After the environment is cleared of the targeted molecule, the sensor returns to its previous electrical baseline as smoke-free air is drawn into the device (bottom figure below) and monitoring continues from the re-established electrical baseline.

Detection of Targeted Molecules and Rejection of Untargeted Molecules

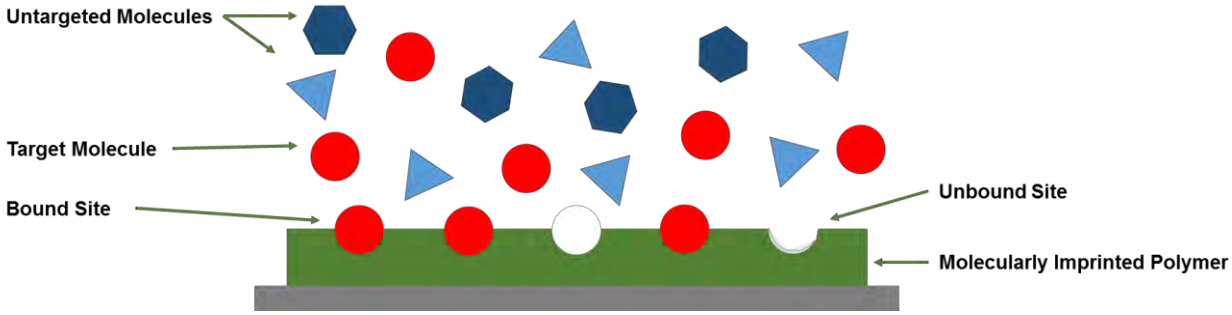

Clearing and Reset After Targeted Molecule No Longer Present

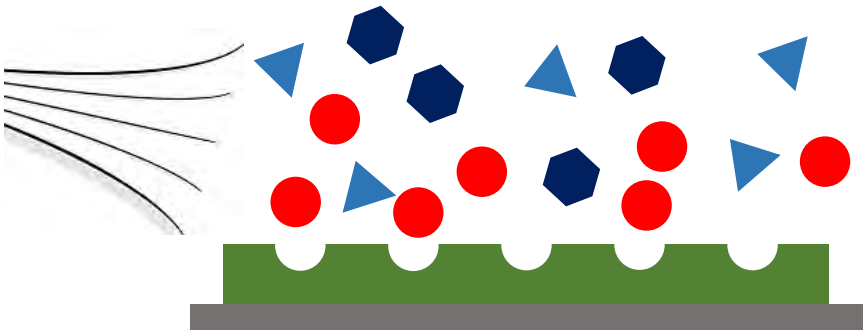

Summary of Expertise and Brief Professional Biography of Dr. J.J. BelBruno:

Dr. BelBruno is one of the foremost experts in molecularly imprinted polymer sensor technology and the inventor of the technology used in FreshAir's sensors. Dr. BelBruno offers a 37-year career as a research chemist. Included in his career are two years as a Research Associate in the Department of Mechanical & Aerospace Engineering at Princeton University, 35 years as a Professor of Chemistry at Dartmouth College and four years as the Chief Technology Officer (CTO) at FreshAir Sensor, LLC. He spent research sabbaticals at the Institute for Physical Chemistry of the Technical University of Munich and in the Department of Physics at the Norwegian National University of Science & Technology in Trondheim. His teaching and research expertise lies on the boundaries among Chemistry, Physics and Engineering. He has published more than 140 peer-reviewed manuscripts in scientific journals and holds 11 patents in the U.S. and Europe. His research most relevant to FreshAir, specifically on molecularly imprinted polymers and sensing devices constructed from those polymers, spans the past 12 years. Dr. BelBruno's complete curriculum vitae is attached.

Dr. BelBruno co-founded FreshAir in 2013 and currently serves as its CTO. He directs a research and development team consisting, at this time, of four chemists and chemical engineers and four hardware and software engineers. FreshAir has a scientific and engineering program for the development of additional sensors and devices. FreshAir's goal is to build sensing devices to protect individuals from exposure to hazardous chemicals in secondhand tobacco and marijuana smoke, provide real-time notification of the presence of these pollutants to improve the local environment and mitigate health effects. Scientific information and details of the testing and operation of FreshAir's devices and sensors are contained in the following pages.

Details on FreshAir's Sensor and Inventor

I. *Additional information on sensor components and operation.*

A reliable, sensitive and specific sensor is essential in a monitoring device for tobacco or marijuana smoke. Recording such exposure in *real time* allows the direct connection of smoke exposure to a particular smoking event. The sensors rely on the properties of electrically conductive polymer materials. These polymers have the electrical properties of metals, but like all polymers, they can be molded and shaped as needed. In the case of the FreshAir sensors, the polymers are processed in the presence of the molecule that is the sensing target and once these target molecules are removed from the polymer, a

binding cavity that is chemically and spatially tuned to the molecule remains. This binding cavity is then able to temporarily capture the target molecule resulting in a measurable change in the electrical properties of the polymer. Conductive polymers are of widespread use industrially as components of electrochemical devices (*i.e*. devices that convert chemical changes into electrical signals) and in applications for a variety of sensing tasks. The sensing applications use the polymers in very thin films, typically of the order of nanometers. Generally, thin film materials are used to optimize the number and availability of target molecule receptor sites, minimize the diffusion distance necessary for the target molecule to travel during binding events, and increase the sensitivity of the sensors.

FreshAir's measurements using conductive polymer films are performed with a planar, chemiresistive structure; the sensor is a chemical resistor in which the value of the electrical resistance depends on the chemical structure of the film. This structure changes temporarily as the target binds to the film. The advantages of such a structure include the rapid measurements that report the presence of secondhand smoke from ambient tobacco or marijuana in *real time*. The sensor consists of the two distinct components: the sensing film and a second, electronic layer that detects the changes in the first film. The second layer is a conductive electrode patterned into an interdigitated grid, which is actually a series of connected electrodes numbering as many as 150 pairs. In operation, these electrodes are constantly monitored for changes by the device's electronics. In trials, the sensing film was sensitive to the number of cigarettes consumed (the number of simultaneously smoked cigarettes), demonstrated recovery between exposures (the signal returned to the baseline between successive exposures to the target) and functioned in the presence of a wide range of exposures to tobacco and marijuana smoke from simulated light-smoking to heavy-smoking environments.

FreshAir's sensors are specifically and proprietarily targeted to particular molecular components of tobacco and marijuana smoke and have undergone extensive testing in our laboratories and our room-sized testing facility. Many thousands of these devices are in use across North America. Typical smoke detectors will be triggered by dust, pollen, smoke, steam, cooking vapors or other types of particles. FreshAir's sensors ignore all of these stimuli and respond only to smoke that contains tobacco or marijuana. The smoke interacts with the polymer-coated sensor developed in FreshAir's laboratories and changes the electrical properties of the sensors contained in the device. After a smoking event, the adsorbed material is eventually removed from the sensors by the smoke-free air passing through the device, and the sensors approximately return to the electrical state (the baseline) that they reported prior to the smoking event, typically within thirty minutes.

The sensors will only detect active smoking in the space in which they are installed; they do not detect smoke infiltrating from other hotel rooms, apartments or hallways, nor will they detect the presence of previous smoking activity. Moreover, the odor that one detects outside of the space in which the smoking occurs is not due to the target molecules.

The data, electrical properties (the changes in resistance of the sensor as a function of time), are constantly monitored, and the data points are stored every fifteen seconds in on-board flash memory and uploaded over Wi-Fi to FreshAir's cloud-based monitoring platform. Data is uploaded to the server every 5 minutes. We monitor the 'health' of our devices which includes their baseline values, the age of the sensors and the number of smoking events a given sensor has reported. In the absence of the target molecules, the electrical properties vary mildly and an approximately constant baseline is observed. When the target molecules are present, a significant change in resistance of the sensors from the baseline is detected by the device's firmware and a message is transmitted notifying FreshAir's cloud-

based monitoring platform and sending an email to the property manager with a Smoking Alert in a format like that shown below.

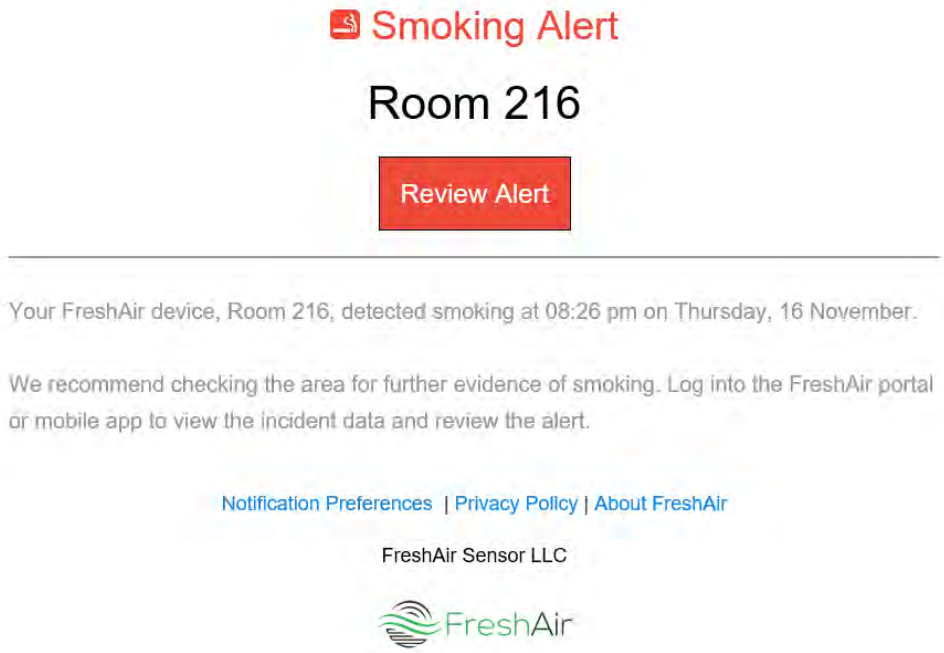

Typical sensor alert email sent to a FreshAir Sensor client.

The property manager is also able to retrieve a graphical representation of the change in resistance (indicating smoking) with a time axis showing the time of the violation and the y-axis showing the evolution of the sensor detection. A typical output is shown in the figure below. The data is also automatically stored in the property manager's account on FreshAir's monitoring platform and can be retrieved at any time.

II. ***Scientific validation of the general principles of detection and the specific sensor.***

The scientific basis of FreshAir's sensing method was peer-reviewed and a manuscript describing the development of the sensor appeared in a high impact journal directed towards researchers active in nicotine and tobacco studies: "Detection of secondhand cigarette smoke via nicotine using conductive polymer films" by Liu, Y., Antwi-Boampong, S., BelBruno, J.J., Crane, M.A., Tanski, S.E. in *Nicotine & Tobacco Research*, (2013) Volume 15, pages 1511-1518.

The experiments described in this manuscript were carried out in a device used in medical research to quantify the amount of nicotine ingested by mice and other animals from controlled cigarette smoke. It is a standard smoking simulator used in medical experiments and the device operated with known concentrations of nicotine generated from burning cigarettes. Examples of the correlation of sensor output with nicotine levels are shown below. Measurements were made at concentrations near 100 parts per billion (Wikipedia describes 1 ppb as approximately 3 seconds in a century).

***Example of graphical representation available to a FreshAir client*: The red line reports the presence of tobacco or marijuana smoke, beginning at 8:14pm, as the deviation from the baseline value. The identity of the smoking material, tobacco or marijuana, is not specified in the stored data or the report. An alert is only sent when the signal meets a stringent set of conditions, including an intensity threshold.**

***Nicotine calibration curve for FreshAir's sensors*: Figure below was reported in the peer-reviewed publication noted in the text above and provides a measure of the capability of the sensors.**

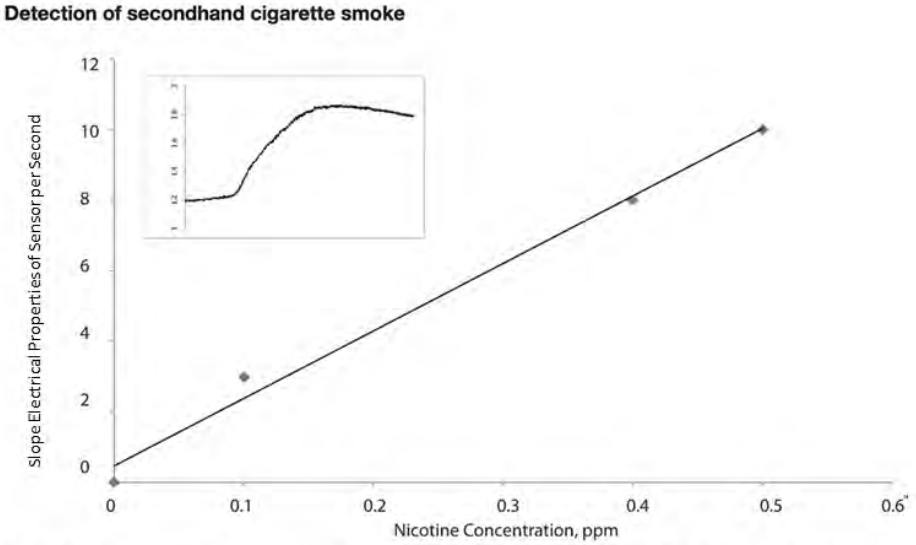

Figure 1. Response of the sensor to vapor-phase nicotine from liquid nicotine at 22 °C. Plot of signal as a function of time for pure nicotine vapor (inset).

III. *Validation of the general technique applied in FreshAir's device.*

The uses of thin film conductive polymers and molecularly imprinted polymers (MIP) in a range of electronic devices are mature, well-understood technologies that are extensively represented in the peer-reviewed scientific literature. A search of that scientific literature indicates that 3,344 manuscripts describing molecularly imprinted polymer sensors have been published in peer-reviewed scientific journals. Moreover, an additional 3,843 peer-reviewed manuscripts involving thin film sensors have been reported in those high impact journals. From the 3,843 published manuscripts, six articles are listed below that review the use of thin films as sensors and provide the usage of these films as representative of the mature state of the technology. Subsequently, eleven published MIP manuscripts from the available 3,344 peer-reviewed reports are listed below to demonstrate the widespread acceptance and maturity of this technology.

Selected thin film sensor scientific review articles: these articles provide the scientific basis and applications of thin polymer films as sensors. The general case for the use of this thin film technology in sensing is strong as evidenced by the number and quality of the scientific reports. This material is very technical.

1. "Conducting polymer based nanobiosensors". Park, C. S.; Lee, C.; Kwon, O. S., *Polymers* (2016), **8**, 249/1-249/18.
2. "Synthesis and sensing applications of polyaniline nanocomposites: a review". Sen, T.; Mishra, S.; Shimpi, N. G., *RSC Advances* (2016), **6**, 42196-42222.
3. "High-performance integrated field-effect transistor-based sensors". Adzhri, R.; Md, M. K.; Gopinath, S. C. B.; Ruslinda, A. R.; Fathil, M. F. M.; Ayub, R. M.; Nor, M. Nuzaihan M.; Voon, C. H., *Analytica Chimica Acta* (2016), **917**, 1-18.
4. "Gas sensors based on electrodeposited polymers". Lakard, B.; Carquigny, S.; Segut, O.; Patois, T.; Lakard, S., *Metals* (2015), **5**, 1371-1386.
5. "Polyaniline-based sensors for gas detection". Yang, S.; Gong, J.; Ohsaka, T., ed. *Trends in Polyaniline Research* (2013), 287-318.
6. "Conducting polyaniline nanowire and its applications in chemiresistive sensing". Song, E.; Choi, J.W., *Nanomaterials* (2013), **3**, 498-523.

Selected molecularly imprinted polymer film sensor scientific review articles: the range of applications of imprinted sensors is vast. These reports provide some indication of the varied targets that can be successfully pursued. Again, these reports are technical.

1. "Recent advances and future prospects in -based electrochemical biosensors". Gui, R.; Jin, H.; Guo, H.; Wang, Z., *Biosensors & Bioelectronics* (2018), **100**, 56-70.
2. "A Review: Electrochemical Sensors for Determination of Biomolecules/Drug". Yola, M. L.; Atar, N., *Current Analytical Chemistry* (2017), **13**, 13-17.
3. "A Review on Synthetic Receptors for Bioparticle Detection Created by Surface-Imprinting Techniques-From Principles to Applications". Eersels, K.; Lieberzeit, P.; Wagner, P., *ACS Sensors* (2016), **1**, 1171-1187.
4. "Evaluating the potential of thermal read-out techniques combined with for the sensing of low-weight organic molecules". van Grinsven, B.; Betlem, K.; Cleij, T. J.; Banks, C. E.; Peeters, M., *Journal of Molecular Recognition* (2017), **30**.
5. "Artificial Biosensors: How Can Sensors Mimic Biorecognition?" Cieplak, M.; Kutner, W., *Trends in Biotechnology* (2016), **34**, 922-941.
6. "Molecular Imprinting: perspectives and applications". Chen, L.; Wang, X.; Lu, W.; Wu, X.; Li, J.,

Chemical Society Reviews (2016), **45**, 2137-2211.
7. “Molecularly imprinted polymers as recognition materials for electronic tongues”. Huynh, T. P.; Kutner, W., *Biosensors & Bioelectronics* (2015), **74**, 856-864.
8. “Molecularly imprinted polymer sensors: realising their potential”. Uzun, L.; Turner, Anthony P. F. *Biosensors & Bioelectronics* (2016), **76**, 131-144.
9. “Recent Innovations of Electrochemical Sensors Based on Electropolymerization Technique”. Peng, Y.; Su, H., *Current Analytical Chemistry* (2015), **11**, 307-317.
10. “Technique for Biosensing and Diagnostics”. Gajovic-Eichelmann, N.; Athikomrattanakul, U.; Dechtrirat, D.; Scheller, F. W., *Springer Series on Chemical Sensors and Biosensors* (2013), **14** (Applications of Nanomaterials in Sensors and Diagnostics), 143-170.
11. “Molecularly imprinted polymers for the Sensing of Explosives and Chemical Warfare Agents” Lu, W.; Xue, M.; Xu, Z.; Dong, X.; Xue, F.; Wang, F.; Wang, Q.; Meng, Z., *Current Organic Chemistry* (2015), **19**, 62-71.

IV. *Quantification of the smoking data.*

FreshAir’s devices do not quantify the amount of smoke in the protected space. FreshAir offers a “smoking/not smoking” type of report. FreshAir has, however, completed quantification tests, and the data are in the peer reviewed manuscript cited above. In addition to in-field tests, FreshAir tests its devices in a room that measures the size of the typical 500 square foot living area or hotel room equipped with ventilation at the standard hotel air turnover rate. In this test facility, smoking event signals are reliably recorded as far as 20 feet from the source of the smoking; a distance that represents the maximum range expected in the typical room of the size noted. FreshAir has conducted more than 16,000 such tests in its testing facility and in clients’ properties. Smoking a single cigarette at this distance reliably and inevitably triggers FreshAir’s sensors under large variations in environmental conditions. Smoking in these tests was monitored over a temperature range from 65°F to 95°F and relative humidity at levels from 20% to 75% to ensure that such changes, possible in a hotel room or an apartment, do not impact the measurements. Other potential environmental interferences were tested. These included more than 30 cleaning products, burning candles, burning incense, cooking in microwave ovens, burning various paper products and open flames. The devices were shown to accurately differentiate smoking from any environmental effects in these tests.

V. *Testing under “real world” conditions.*

The device is installed by the client and FreshAir monitors remotely to confirm which signals are due to smoking. The device cannot be incorrectly installed. The client is guided through installation by the instructions in the installation application on a mobile device. The sensor responds to installation commands by a series of different color LED flashes. If installation is unsuccessful, both the device and the app will so indicate and ask the user to re-initialize. Similarly, the baseline signal is automatically calculated by the firmware and the monitoring software eliminating the possibility of error, human or otherwise. Based on the results from the testing facility and clients’ properties, minimum standards were set for reporting an event as smoking. Those standards include: the signal exceeding a threshold for the tobacco and marijuana signal, the signal exhibiting a well-defined rise time, confirming any changes in environmental conditions or secondary indicators and confirming that the sensors are functional and within operational limits. In order to filter out potential false positives, FreshAir has established extremely conservative criteria for reporting an event as a smoking event.

Real world testing data is related to the outcomes reported to us by clients. FreshAir has completed thousands of tests in its testing facility but also has client-confirmed data. The best data from clients

involves confirmation of forwarded smoking alerts. For example, one of FreshAir's clients, a 400-room hotel, responds to Smoking Alerts by immediately knocking on the door of the room where the violation has occurred. In October 2017, FreshAir delivered 78 Smoking Alerts to this client. Nearly all of the alerts were confirmed and the hotel occupants were charged a smoking fine and/or asked to leave. The remaining alerts were not acted upon by the hotel staff. FreshAir's range of data from testing and device use includes over 1 billion elements.

VI. ***Maintenance standards/confirming functionality.***

As noted, we set extremely conservative criteria to be met before any event is considered smoking and an alert generated including minimum changes in the detected resistance. This is to ensure the absence of false positives (most likely creating a small number of false negatives). We have tested against a range of potential interfering substances by recording the baseline signal and spraying/wiping with the these potential interferents. Any signal generated by these materials exhibits different signatures from tobacco or marijuana. We also include temperature and humidity sensors in the device to account for any possible signal due to these environmental factors and we include a reliable secondary indicator of smoking to discriminate against any spurious signal. Changes in temperature and/or humidity cause small (~1%) changes in the resistance output of the tobacco/marijuana sensors. To ensure that the device is operating properly, we examine the device output over the previous 24 hours. This small, cyclic variation with the temperature is assurance that the device is functional and that the reported signal is due to smoking.

VII. ***Data validation.***

FreshAir's in-house testing, over more than 30,000 tests, defined results that are consistent with a smoking event and, therefore, not attributable to any other interpretation. FreshAir has the signatures of other substances that could be present as well as the data from the ancillary sensors in its device and can distinguish non-smoking events from smoking events. The data which is supplied to the client shows the sensor levels for at least one hour prior to the smoking event, providing a baseline response in the absence of smoking. If requested, the client will be supplied with standard event curves from in-house testing as a comparison point for a smoking event

Curriculum Vitae

JOSEPH J. BELBRUNO
+1-603-643-7181
info@freshairsensor.com

Professional Background:

2013-	Founder and Chief Technology Officer, FreshAir Sensor LLC
1994-	Professor, Department of Chemistry, Dartmouth College
1998-2001	Chair, Department of Chemistry, Dartmouth College
1988-1994	Associate Professor, Department of Chemistry, Dartmouth College
1982-1988	Assistant Professor, Department of Chemistry, Dartmouth College
1980-1982	Research Associate, Department of Chemistry, Princeton University
1981	Visiting (Laboratory) Astronomer, Kitt Peak National Observatory

Education:

1980	Rutgers University, Ph.D.
1974	Seton Hall University, B.S. (Magna cum laude)

Research Experience:

Current	*Materials and Sensors, Computational Chemistry, Surface-Gas Interactions, Thin Film Deposition, Molecularly Imprinted Polymers*
1980-1982	*Chemical Dynamics of Rotational Energy Transfer and Laser Spectroscopy*, with Professor Herschel Rabitz (Princeton)
1976-1980	*Molecular Beam Studies of Electronic Energy Transfer between Atoms and Molecules*, with Professor John Krenos (Rutgers)
1974-1976	*Analytical Chemistry*, Research Chemist with American Cyanamid Co.

Awards:

2012	Visiting Professor, Physics Dept. NTNU, Trondheim, NO
2011	Arts & Sciences Graduate Faculty Mentoring Award
1998	Fellow, Dartmouth Humanities Institute (Ethics and the Internet)
1988	Alexander von Humboldt Fellow (Technische Universität München)
1986	Dartmouth Faculty Fellow
1977	Johnson & Johnson Fellow
1973	ACS Summer Fellow

Professional Societies:

American Chemical Society
Materials Research Society
von Humboldt Society
Society of Sigma XI

Currently Active Research:

Development of Sensors
Nanotechnology/Nanochemistry
Computational Studies of Surface-Gas Processes
Studies of Semiconductor NanoCluster Deposition
Experimental/Computational Studies of Molecular Imprinting

Synergistic Activities:
Service: Member of EPA Peer Consultation on Materials Characterization of Nanoscale Materials; Member of NSF Review Panel for Graduate Fellowships; Member of DoD Review Panel for Graduate Fellowships

Member of the Editorial Board of the journal *Nanomaterials*, Executive Editor of *Journal of Basic & Applied Sciences* and Associate Editor of the journal *Chemical Sensors*

Education: Development of the Materials Ph.D. track within Chemistry; Presenter/Mentor for local seminar on applying for NSF Graduate Fellowships

Computing Issues: Member of the Advisory Board for the Institute for Security and Technology Studies (2003-2006)-this is a separate, US funded research center located at Dartmouth College.
Scientific Ethics: Developed case-based course for summer REU program; participant in the incoming graduate student "Ethics in Research" training.

Collaborators:
Dartmouth: Susanne Tanski (Medical School), Mardi Crane (Medical School)

External: Asta Richter (TFH-Wildau), Roger Smith and Steven Kenny (Loughborough, UK), Stefan Bromley (Barcelona), Ursula Gibson (Trondheim), Scott Woodley (London, UK)

Graduate Students and Postdoctoral Associates:
Postdocs (previous): Zichao Tang, Guanming Wang, Guandong Zhang

Ph.D. Graduate Students (current): Alyson Michael, Holger Moustakas

Ph.D. Graduate Students (previous): Yuan Liu, Sadik Antwi-Boampong, April Daigle, Sara Campbell, Andrei Burnin, Ed Sanville, Krum Chuchev, Yinghua Shen, Elizabeth Christophy, Jimmy Tung, David Morriseau (MS), George Raiche, Gary Siuzdak, Jinpeng Lv, Ziyi Chai, Stefano Poggio

Advisors:
Ph.D. Thesis: John Krenos (Rutgers University)
Postdoctoral: Herschel Rabitz and Richard Miles (Princeton University)

Textbook:
D. Wallace and J.J. BelBruno, *The Bell That Rings Light: An Introductory Text in Quantum Mechanics.* World Scientific Publishing. (2006).

Patents Issued:
1. J.J. BelBruno, U.J. Gibson, J.E.G. Lipson and M.N. Wybourne, "Molecularly imprinted polymer sensor systems and related methods". US Patent No. 9,034,262 (May 19, 2015).
2. J.J. BelBruno, "Molecularly imprinted polymers for detection of contaminants". US Patent No. 9,228,988 (January 5, 2016).
3. Z.R. Greenhill, J.J. BelBruno and Y. Avniel, "Composite material". US Patent No. 9,060,560 (June 23, 2015).
4. Z.R. Greenhill, J.J. BelBruno and Y. Avniel, "Gradient nanoparticle carbon allotrope polymer composite material". US Patent No. 9,328,788 (May 3, 2016).
5. Z.R. Greenhill, J.J. BelBruno and Y. Avniel, "Composite material". Canadian Patent No. 2696048 (May 3, 2016).
6. J.J. BelBruno and M. Kelm, "Molecularly imprinted polymer for wine, method of preparing, and use of same". US Patent No. 9,260,683 (February 26, 2016).
7. Z.R. Greenhill, J.J. BelBruno and Y. Avniel, "Composite material". Israeli Patent No. 203875 (July 1, 2016).
8. Z.R. Greenhill and J.J. BelBruno, "Gradient nanoparticle-carbon allotrope-polymer composite material". European Patent No. EP2629973 (September 11, 2016).
9. J.J. BelBruno and S. Tanski, "Airborne contaminant sensor device and method for using the same" US Patent No. 9,429,536 (August 30, 2016).
10. A. Burnin and J.J. BelBruno, "Electronic time-of-flight mass selector", U.S. Patent No. 7,829,843 (November 9, 2010).
11. Z.R. Greenhill, J.J. BelBruno and Y. Avniel, "Composite material". Great Britain Patent No. 2519458 (September 1, 2016).

12. J.J. BelBruno, “Methods for preparation of molecularly imprinted polymers for wine extraction”, U.S. Patent No. 10,000,598 (June 19, 2018).
13. J.J. BelBruno, “Molecularly imprinted polymer sensors”, U.S. Patent No. 10,024,814 (July 17, 2018.
14. A. Barnes and J.J. BelBruno, “Food allergen detection methods and systems using molecularly imprinted polymers”, U.S. Patent No. 10,107,819 (October 23, 2018).
15. J.J. BelBruno and S. E. Tanski, “Devices for detecting airborne contaminants and associated methods”, U.S. Patent No. 10,451,598 (October 22, 2019).

Publications:

1. J.J. BelBruno, “Clusters and Nanoparticles: The Experimental-Computational Connection to Understanding”. Invited chapter in the monograph: “***Computational Modelling of Nanoparticles”***, edited by S. Bromley and S. Woodley. 171-188*,* (2018) Elsevier.
2. J.J. BelBruno, “Molecularly Imprinted Polymer Sensors“. Invited manuscript, *Chemical Reviews*, **119**, 94-119 (2019).
3. J.J. BelBruno, “Conducting Polymeric Materials for Sensing”, *Science Advances Today*, **2**, 25251-25262 (2016)
4. E.A. Karhu, C.R. Ildstad, S. Poggio, V. Furtula, N. Tolstik, I.T. Sorokina, J.J. BelBruno, and U.J. Gibson, “Vapor deposited Cr-doped ZnS thin films: towards optically pumped mid-infrared waveguide lasers” *Optics Materials Express*, **6,** 2947-2955 (2016).
5. A. Burnin, S. Poggio, J. King and J.J. BelBruno, “Direct growth by arc discharge and computational study of zinc sulfide nanotubes” *Journal of Materials Science***, 51**, 9716-9722 (2016).
6. S. Poggio, B. Wang, U.J. Gibson and J.J. BelBruno. “Properties of transition metal substituted zinc sulfide hexamers and dodecamers”, *Phys. Chem. Chem. Phys.*, **17,** 14208-14214 (2015).
7. Z. Chai and J.J. BelBruno, “Thermochemical study of amino acid imprinted polymer films”, *J. Molecular Recognition*, **28**, 651-655 (2015).
8. N.A. Molland, Z. Ghadyani, E.A. Karhu, S. Poggio, M. Nematollahi, M. Kildemo, T.W. Reenaas, J. J. BelBruno and U. J. Gibson, “Band-edge modification and mid-infrared absorption of co-deposited $Fe_xZn_{1-x}S$ thin films”, *Optics Materials Express*, **5,** 1613-1620 (2015).
9. A. Burnin, J.J. BelBruno and U.J. Gibson, “Evidence of chromium-cobalt binary cluster formation by pulsed laser evaporation”, *Int. J. Mass Spectrom.* **380**, 7-11 (2015).
10. S. Antwi-Boampong, J.S. Peng, J. Carlan and J.J. BelBruno, “A molecularly imprinted fluoral-p/polyaniline double layer sensor system for selective sensing of formaldehyde”, *Sensors Journal, IEEE* **14**, 1490-1498 (2014).
11. J.J. BelBruno, “Nanomaterials in Sensors”, *Nanomaterials* **3**, 572 (2013).
12. Sadik Antwi-Boampong, Kristina Mani, Jean Carlan and Joseph J. BelBruno, “A selective molecularly imprinted polymer-carbon nanotube sensor for cotinine sensing.”*Journal of Molecular Recognition* **27**, 57-63 (2014).
13. Jinpeng Lv, Chundong Li, and J. J. BelBruno. "Defect evolution on the optical properties of H+-implanted ZnO whiskers." *CrystEngComm* **15,** 5620-5625 (2013).
14. Jinpeng Lv, Chundong Li, and J. J. BelBruno. "Characteristics of point defects on the optical properties of ZnO: revealed by Al–H co-doping and post-annealing." *RSC Adv.* **3**, 8652-8656 (2013).
15. Sadik Antwi-Boampong, Yuan Liu, Asta Richter, and Joseph J. BelBruno. "Effect of the host polymer on the nanomechanical and morphological properties of templated polymer films." *Journal of Applied Polymer Science* **130**, 877-883 (2013).
16. Sadik Antwi-Boampong and Joseph J. BelBruno. "Detection of formaldehyde vapor using conductive polymer films." *Sensors and Actuators B* **182**, 300-306 (2013).
17. Y. Liu, S. Antwi-Boampong, J.J. BelBruno, M.A. Crane and S.E. Tanski*,* “Detection of secondhand cigarette smoke via nicotine using conductive polymer films” *Nicotine & Tobacco Research* (2013); doi: 10.1093/ntr/ntt007.
18. S.W.R. Dunbar and J.J. BelBruno, “Molecularly imprinted polymer-carbon nanotube sensor targeted to cotinine”, Chemical Sensors, **2**, 14 (2012).
19. A.D. Lewoczko, A.D., J.J. BelBruno and S.T. Bromley, "Effect of spin ordering on structure and structural transitions in the $(MnS)_6$ magic cluster." *Chem. Phys. Lett.* **556**, 207 (2012).
20. A.D. Lewoczko and J.J. BelBruno, "Impact of surface steps and oxygen pre-coverage on the adsorption of methylamine on gold." *Phys. Chem. Chem. Phys.* **15**, 4707 (2013).
21. G. Giacomo, A.D. Lewoczko, J.J. BelBruno and S.T. Bromley, "Interplay between Magnetism and Magic-ness in Nanoclusters." *J. Phys. Chem. C* **116**, 20625 (2012).
22. A. Daigle and J.J. BelBruno, “Density Functional Theory Study of the Adsorption of Nitrogen and Sulfur

Atoms on Gold (111), (100), and (211) Surfaces", *J. Phys. Chem. C*, **115**, 22987 (2011).
23. A. Daigle and J.J. BelBruno, "Density functional theory study of the adsorption of oxygen atoms on gold (111), (100) and (211) surfaces", *Surface Science* **605**, 1313 (2011).
24. A. Richter and J.J. BelBruno, "Characterization of functional states in nicotine- and cotinine-imprinted poly(4-vinylphenol) films by nanoindentation", *J. Applied Polymer Science,* **124**, 2798 (2012).
25. J.J. BelBruno, G. Zhang and U.J. Gibson, "Capacitive sensing of amino acids in molecularly imprinted nylon films", *Sensors and Actuators B* **155**, 915 (2011).
26. J. J. BelBruno and A. Burnin, "Small germanium sulfide clusters: mass spectrometry and density functional calculations", *Phys. Chem. Chem. Phys.* **12**, 8557 (2010).
27. J.J. BelBruno, "Molecularly Imprinted Polymers: Artificial Receptors with Wide-Ranging Applications", *Micro and Nanosystems,* **1**, 163 (2009).
28. J. J. BelBruno, E. Sanville, A. Burnin, A. K. Muhangi and A. Malyutin, "Structural Calculations and Experimental Detection of Small Ga_mS_n Clusters Using Time of Flight Mass Spectrometry", *Chem. Phys. Lett.* **478**, 132 (2009).
29. S.E. Campbell, M. Collins, Lie Xie, Lei and J.J. BelBruno "Surface morphology of spin-coated molecularly imprinted polymer films", *Surface and Interface Analysis* **41**, 347 (2009).
30. J.J. BelBruno, A. Richter and U. Gibson, "Amazing pores: processing morphology and functional states of molecularly imprinted polymers as sensing materials", *Molecular Crystals and Liquid Crystals* **438**, 179 (2008).
31. K. Chuchev and J.J. BelBruno, "Oxidation of catechol to 2-hydroxymuconic semialdehyde", *THEOCHEM* **856**, 71 (2008).
32. J.J. BelBruno, "Adsorption of ZnO, $(ZnO)_2$ and $(ZnO)_3$ on MgO(001).", *Surface Science* **602** 1837 (2008).
33. K. Chuchev and J.J. BelBruno, "Computational treatment of the microsolvation of neutral and zwitterionic forms of alanine", *THEOCHEM* **850**, 111 (2008).
34. S.E. Campbell and J.J. BelBruno, "Nanoindentation study of thin film molecularly imprinted polymers", Abstracts of Papers, 235th ACS National Meeting, New Orleans, LA, United States, April 6-10, 2008 (2008).
35. R. Smith, S.D. Kenny, J.J. BelBruno and R.E. Palmer, "Modelling the structure and dynamics of metal atom nanoclusters deposited on graphite", *Chemical Physics of Solid Surfaces* **12**, 589 (2007).
36. E. Sanville and J.J. BelBruno, "Electronic and geometric structure calculations of adsorption of small $(ZnO)_i$ clusters (i=1-4) on graphite", *Physical Review B* **76**, 085412 (2007).
37. A. Richter, H. Gojzewski and J.J. Belbruno, "Visco-elastic properties of thin nylon films using multi-cycling nanoindentation" *Int. J. Materials Research* **98**, 414 (2007).
38. K. Chuchev and J.J. BelBruno, "Mechanisms of decarboxylation of ortho-substituted benzoic acids", *THEOCHEM* **807**, 1 (2007).
39. J.J. BelBruno, A. Richter, S.E. Campbell and U.J. Gibson, "Detection of functional states of molecularly imprinted thin films with multi-cycling nanoindentation", *Polymer,* **48**, 1679 (2007).
40. A. Richter, U.J. Gibson, M. Nowicki and J.J. BelBruno, "Processing and morphology of molecularly imprinted nylon thin films", *J. Appl. Polym. Sci*, **101**, 2919 (2006).
41. A. Richter, M. Gruner, J.J. BelBruno, U.J. Gibson and M. Nowicki, "Nanomechanical measurements on glutamine molecularly imprinted nylon films", *Colloids and Surfaces, A* **284/285**, 401 (2006).
42. K. Chuchev and J.J. BelBruno, "Theoretical study of carboxylic acids with explicit water molecules", *THEOCHEM* **763**, 199 (2006).
43. R. Smith, C. Nock, S. D. Kenny, J.J. BelBruno, M. Di Vece, S. Palomba and R.E. Palmer, "Modeling the pinning of Au and Ni clusters on graphite", *Physical Review B: Condensed Matter and Materials Physics*, **73**, 125429 (2006).
44. K. Chuchev and J.J. BelBruno, "Oxidation of catechol to muconic acid: A theoretical study", *THEOCHEM*, **761**, 209 (2006).
45. E. Sanville and J.J. BelBruno, "Adsorption of $(ZnS)_i$ (i=1-4) clusters on graphite surfaces", *Physical Review B: Condensed Matter and Materials Physics*, **73**, 085416 (2006).
46. K. Chuchev and J.J. BelBruno, "Rotation barriers in condensed rings: an extension of Clar's stability rule", *Journal of Physical Organic Chemistry*, **19**, 115 (2006).
47. E. Sanville, A. Burnin and J.J. BelBruno, "Experimental and Computational Study of Small (n = 1-16) Stoichiometric Zinc and Cadmium Chalcogenide Clusters", *Journal of Physical Chemistry A*, **110**, 2378 (2006).
48. Y. Shen and J.J. BelBruno, "Studies of Neutral and Ionic CuAr and CuKr van der Waals Complexes", *Journal of Physical Chemistry A*, **109**, 10077 (2005).
49. A. Burnin, E. Sanville and J.J. BelBruno, "Experimental and Computational Study of the Zn_nS_n and $Zn_nS_n^+$ Clusters", *Journal of Physical Chemistry A*, **109**, 5026 (2005).

50. Y. Shen and J.J. BelBruno, “Density Functional Theory Study of the Jahn-Teller Effect and Spin-Orbit Coupling for Copper and Gold Trimers”, *Journal of Physical Chemistry A*, **109**, 512 (2005).
51. G.M. Wang, J.J. BelBruno, S.D. Kenny and R. Smith, “Density functional study of Au_n (n = 3-5) clusters on relaxed graphite surfaces”, *Surface Science*, **576**, 107 (2005).
52. K. Chuchev and J.J. BelBruno, “Small, Nonstoichiometric Zinc Sulfide Clusters”. *Journal of Physical Chemistry A*, **109**, 1564 (2005).
53. J.J. BelBruno, “Half-sandwich metal atom complexes with benzene: a model for adsorption onto graphite”, *Surface Science*, **577**, 167 (2005).
54. K. Chuchev and J.J. BelBruno, “Density Functional Theory Study of the Isomers of C_nB and C_nB_2”, *Journal of Physical Chemistry A*, **108**, 5226 (2004).
55. G.M. Wang, J.J. BelBruno, S.D. Kenny and R. Smith, “Gold adatoms and dimers on relaxed graphite surfaces”, *Physical Review B*, **69**, 195412/1 (2004).
56. Maier, J. Werner-Allen, U.J. Gibson, A. Richter, J.J. BelBruno, “Scanning force microscopy study of the morphology of spin-cast molecular-imprinted nylon thin films”, *Surface and Interface Analysis*, **36**, 1340 (2004).
57. E. Sanville and J.J. BelBruno, “Computational studies of possible transition structures in the insertion and windowing mechanisms for the formation of endohedral fullerenes”, *J. Phys. Chem. A*, **107**, 1887 (2003).
58. K. Chuchev and J.J. BelBruno, “DFT study of the electronic state, geometry and harmonic frequencies for linear C_nP_2 clusters; a comparison with C_nN_2”, *J. Phys. Chem. A*, **107**, 11217 (2003).
59. Y. Shen and J.J. BelBruno, “Ag_3 Born-Oppenheimer potential hypersurfaces”, *J. Chem. Phys*., **118**, 9241 (2003).
60. A. Burnin and J.J. BelBruno, “SC_nS linear chain production by direct laser ablation”, *J. Phys. Chem. A*, **107**, 9547 (2003).
61. R. Smith, S.D. Kenny, C.F. Sanz-Navarro and J.J. BelBruno, “Nanostructured surfaces described by atomistic simulation methods”, *J. Phys. C*,**15**, S3153 (2003).
62. A. Richter, B. Wolf and J.J. BelBruno, “Investigation of semiconductors by nanoindentation”, *Solid State Phenomena*, **95-96**, 519 (2003).
63. G. Wang, J.J. BelBruno, S.D. Kenny and R. Smith “Interaction of silver adatoms and dimers with graphite surfaces”, *Surface Science* **541**, 91 (2003).
64. K. Chuchev and J.J. BelBruno, “Elecrtronic structure of C_5N_2, C_6N_2 and isoelectronic molecules” *J. Phys. Chem. A,* **107**, 1887 (2003).
65. J.J. BelBruno, “Bonding and energetics in small gallium-arsenide clusters”, *Heteroatom. Chem.,* **14**, 189 (2003).
66. A. Burnin and J.J. BelBruno, “$Zn_nS_m^+$ cluster production by laser ablation”, *Chem. Phys. Lett.*, **362**, 341 (2002).
67. J. J. BelBruno, “Computational study of $N@C_{60}$, $P@C_{60}$ and $As@C_{60}$”, *Fullerenes, Nanotubes and Carbon Nanostructures*, **10**, 23 (2002).
68. K. Crabb, N. Shneskoff and J.J. BelBruno, “An improved molecularly imprinted polymer film for recognition of amino acids”, *J. Appl. Polym. Sci.* **86**, 3611 (2002).
69. K. Chuchev and J.J. BelBruno, “Density Functional Theory Study of the Isomers of C_6N” *J. Phys. Chem. A* **106**, 4240 (2002).
70. P.D. Godwin, S.D. Kenny, R. Smith and J.J. BelBruno, “The structure of C_{60} and endohedral C_{60} on the Si{1 0 0} surface” *Surface Science* **490**, 409 (2001).
71. Z. Tang and J.J. BelBruno, “Structures and energies of C_nS^+ ($1 \le n \le 16$) and C_nS^- ($9 \le n \le 16$) clusters” *International Journal of Mass Spectrometry* **208**, 7 (2001).
72. J.J. BelBruno, Z.C. Tang, R. Smith and S. Hobday, “The structure and energetics of carbon-nitrogen clusters” *Molecular Physics* **99**, 957 (2001).
73. J. Ni and J.J. BelBruno, “MOCVD of cadmium and gallium using metastable atom energy transfer” *Materials Letters* **49**, 75 (2001).
74. Stefan Andreev and Joseph J. BelBruno, “Detection of AuF by emission spectroscopy in a hollow cathode discharge” *Chemical Physics Letters* **329**, 490 (2000).
75. Z. Tang, J.J. BelBruno, R. Huang and L. Zheng, " Collision-induced dissociation and density functional study of the structures and energies of cyclic $C_{2n}N_5^-$ clusters", *J. Chem. Phys.* **112**, 9276 (2000).
76. J.J. BelBruno, "The structure of small GaN clusters ", *Heteroatom Chemistry* **11**, 281 (2000).
77. R. Smith, K. Beardmore and J.J. BelBruno, "H-C_{60} and Low Energy H Impact with Fullerite", *J. Chem. Phys.* **111**, 9227 (1999).
78. S. Hobday, R. Smith and J.J. BelBruno, "Applications of Neural Networks to Fitting Interatomic Potential Functions", *Modell. Simul. Mater. Sci. Eng.*, **7**, 397 (1999).
79. D. Sponholtz, J. Tung, M. Walters and J.J. BelBruno, "A Simple, Efficient Ozone Generator", *J. Chem. Educ.*, **76**, 1712 (1999).

80. A. Sandoski and J.J. BelBruno, "Photochemistry and Photophysics of Small Heterocyclic Molecules: III. cw IR Laser Induced Reaction of Ethylene Oxide", *J. Phys. Org. Chem.* **12**, 681 (1999).
81. J.J. BelBruno, "The Structure of Aluminum Nitride Clusters: A DFT Study", *Chem. Phys. Lett.* **313**, 795 (1999).
82. R. Smith, S. Hobday and J.J. BelBruno, "Applications of Genetic Algorithms and Neural Networks to Interatomic Potentials", *Nucl. Instrum. Methods Phys. Res., B*, **153**, 247 (1999).
83. J.J. BelBruno, "The Application of Density Functional Theory to Metal-Containing Radicals: A Study of the Organometallic Radicals GeH, $GeCH_3$ and GeC_2H_5", *Faraday Transactions* **94**, 1555 (1998).
84. J.J. BelBruno, "The Application of Effective Core Potentials in Heavy Atom Molecules: A Study of Au_2 and CH_3AuPH_3 as a Function of Theoretical Method", *Heteroatom Chemistry* **9**, 651 (1998).
85. J.J. BelBruno, "Ab initio Calculations of the Structures and Energies of Gas Phase Isomeric C_3N_4 Molecules", *Chem.Phys. Lett.* **270**, 99 (1997).
86. J.J. BelBruno, "Ab initio Calculations of the Structures and Energies of $Ge(CH_3)_2$ from Tetramethylgermane in CVD", *Heteroatom Chemistry*, **9**, 195 (1998).
87. J.J. BelBruno, (Book Review) Processes and Problems in Atmospheric Chemistry *J. Am. Chem. Soc.* **119**, 6454 (1997).
88. J. Ni and J.J. BelBruno, "Mechanistic Details for CdS Production by MOCVD", *J. Crystal Growth*, **182**, 321 (1997).
89. J.J. BelBruno, "Ab initio Calculations of the Rotational Barriers in H_2Te_2 and $(CH_3)_2Te_2$", *Heteroatom Chemistry* **8**, 199 (1997).
90. J.J. BelBruno, "Ab initio Calculations of the Ring-opened and Ring-closed Isomers of $C_2H_4O^{\bullet+}$: The Need for High Level Electron Correlation Techniques", *Chem. Phys. Lett.*, **263**, 84 (1996).
91. J.J. BelBruno, "Ab initio Calculations of the Potential Energy Surfaces for the Unimolecular Dissociation Reactions of Ethylene Oxide", *J. Phys. Org. Chem.* **10**, 113 (1997).
92. J.J. BelBruno, "Ab initio Calculations of the Energies of the Ring-opened and Ring-closed Isomers of $C_2H_4S^+$, *Chem. Phys. Lett.* **254**, 321 (1996).
93. A. Sandoski and J.J. BelBruno, "Absorptivity of SiF_4 at $1027cm^{-1}$ for High cw-Laser Power", *Appl. Spec.* **50**, 420 (1996).
94. J.J. BelBruno, "Ab initio Calculations of the Rotational Barrier in Dimethyl Diselenide", *Heteroatom Chemistry* **7**, 39 (1996).
95. D.M. Stearns, J.J. BelBruno and K.E. Wetterhahn, "A Prediction of Chromium(III) Accumulation in Humans from Chromium Dietary Supplements", *FASEB J.* **9**, 1650 (1995).
96. J.J. BelBruno and R. Quinney, "Chemiluminescence from the MPD of Organomettalic Iron Complexes" *Spectroscopy Lett.* **29**, 41 (1995).
97. J.J. BelBruno, "Molecular Orbital Calculations of the Rotational Barrier in Benzeneselenenyl Molecules", *J. Molec. Struct.* **358**, 125 (1995).
98. J.J. BelBruno, "Molecular and Electronic Structure of Benzeneselenenyl Molecules and Cations", *Heteroatom Chemistry* **6**, 499 (1995).
99. J.J. BelBruno, "Multiphoton Spectroscopy and Chemical Dynamics" *International Reviews in Physical Chemistry* **14**, 67 (1995).
100. M. Antman, E. Christophy and J.J. BelBruno, "MPI Spectroscopy of Germanium Atoms Produced by Multiphoton Dissociation of $Ge(C_2H_5)_4$", *Chem. Phys. Lett..* **221**, 294 (1994).
101. J.J. BelBruno, "A Experimental/Theoretical Comparison of the Non-Resonant Multiphoton Ionization Fragmentation Mechanisms for Heterocycles and the Corresponding Acyclic Molecules" *Int. J. Mass Spectrom. Ion Processes*, **139**, 1 (1994).
102. J.J. BelBruno, "Lasers in the Physical Chemistry Curriculum", *J. Chem. Ed.*, **71**, 309 (1994).
103. J.J. BelBruno, "Non-resonant Multiphoton Ionization of Cyclopentane and its Heterocyclic Analogues", *Appl. Phys.***B56**, 263 (1993).
104. G. Gribble, D. Keavy, D. Davis, M. Saulnier, M. Sibi, B. Pelcman and J.J. BelBruno, "Synthesis and Diels - Alder Cycloaddition Reactions of 4H-Furo[3,4-6]indoles. A regiospecific Diels-Alder Synthesis of Ellipticine",*J. Org. Chem.* **57**, 5878 (1992).
105. J.J. BelBruno, "MPD Dynamics of Organoiron and Organoselenium Molecules", in*Laser Chemistry of Organometallics*, 49 (1993).
106. J.J. BelBruno, "Laser Photo-oxidative Chemistry of Quadricyclane", *Physical Chemistry: Developing a Dynamic Curriculum*, American Chemical Society: 1993 (Chapter 10).
107. J.J. BelBruno, "Nonlinear Photochemistry", *Research Trends in Physical Chemistry*, **2**, 185 (1992).

108. J.J. BelBruno and E. Christophy, "Non-resonant Multiphoton Ionization of Small Cyclic Molecules: A Comparison of Stable and Metastable Fragmentation Pathways for Ethylene Sulfide, Ethylene Oxide, Propylene Oxide and Cyclopropane", *Int. J. Mass Spectrom. Ion Processes*, **115**, 111 (1992).
109. B. Ernstberger, H. Krause, A. Kiermeier, J.J. BelBruno and H.J. Neusser , "A Comparison of the Ionization Potentials for the Benzene, p-Difluorobenzene and Benzene/p-Difluorobenzene Dimers", *J. Chem. Phys.*, **95**, 3302 (1991).
110. G. Siuzdak, S. North and J.J. BelBruno, "Multiphoton Ionization of Phenol in Non-Aqueous Solution: Characterization of the Cation and Ion-Molecule Chemistry", *J. Phys. Chem.* **95**, 5186 (1991).
111. G. Siuzdak and J.J. BelBruno, "Multiphoton Ionization of Nitrobenzene in Non-Aqueous Solution: Characterization of the Cation and Ion-Molecule Chemistry", *Laser Chem.* **11**, 83 (1991).
112. J.J. BelBruno, J. Spacek and E. Christophy, "Multiphoton Dissociation Dynamics of Dimethylselenide", *J. Phys. Chem.*, **95**, 6928 (1991).
113. J.J. Belbruno and G. Siuzdak, "Resonant Ionization in Solution: Initiation of Ion-Molecule Chemistry by REMPI", in *Resonance Ionization Spectroscopy 90*, Inst. Phys. Conf. Ser. **114**, 351 (1991).
114. J.J. Belbruno and G. Siuzdak, "REMPI-MS: Application to the Study of the Gas Phase Dynamics of Radical Cations", in *Resonance Ionization Spectroscopy 90*, Inst. Phys. Conf. Ser. **114**, 177 (1991).
115. G. Siuzdak and J.J. BelBruno, "Multiphoton Ionization Studies of Amines with uv-vis Lasers", *Applied Physics B* **50**, 221 (1990).
116. G. Siuzdak and J.J. BelBruno, "Laser Multiphoton Dissociation/Ionization of Butylamines: Competitive Processes in Radical Cations", *J. Phys. Chem.* **94**, 4559 (1990).
117. J.J. BelBruno, G. Siuzdak and S. North, "Multiphoton Induced Chemistry of Phenol in Hexane at 266 nm", *Chem. Phys. Lett.* **166**, 167 (1990).
118. J.J. BelBruno, G. Siuzdak and S. North, "UV-Multiphoton Induced Ion-Molecule Chemistry of Nitrobenzene in Solution", *Laser Chem.* **10**, 177 (1990).
119. J.J. BelBruno, "The Mechanism of the Fragmentation of Organometallic Complexes via Multiphoton Pumping", *Chem. Phys. Lett.* **160**, 267 (1989).
120. G.A. Raiche and J.J. BelBruno, "Laser Ionization Spectroscopy of Octafluorocyclooctatetraene", *Spec. Lett.* **22**, 747 (1989).
121. J.J. BelBruno and J. Campbell, "Photochemistry and Photophysics of Small Heterocyclic Molecules: II. cw IR Laser Enhancement of the Bimolecular Reaction of Thiirane", *J. Phys. Chem.* **93**, 4005 (1989).
122. J.J. BelBruno, (Book Review) *Gas-Phase Chemiluminescence and Chemi-ionization*, *J. Am. Chem. Soc.* **110**, 6281 (1988).
123. J.J. BelBruno and G.A. Raiche, "Laser-Assisted Chemistry in the Reaction of Mg(^{1}S) with CO_2 to Yield MgO(B^1S^+)", in *Advances in Laser Science III*, W.C. Stwalley and J. Gole, ed. (1988).
124. G.A. Raiche and J.J. BelBruno, "Evidence for Laser-Assisted Chemistry in the Reaction Mg(^{1}S) + $CO_2(^1S_g^+) \rightarrow$ MgO (B^1S^+) + CO", *Chem. Phys. Lett.* **146**, 52 (1988).
125. J.J. BelBruno, S.R. Greenfield, R.T. Carl and R.P. Hughes, "Competition among Collisional Deactivation, Ionization and Dissociation in the Multiphoton Excitation of Octafluorocyclooctatetraene", *J. Phys. Chem.* **92**, 2480 (1988).
126. J.J. BelBruno, P.B. Kobsa, R.T. Carl and R.P. Hughes, "Competition between Radiative Pumping and Nonradiative Processes in the Multiphoton Dissociation of Organometallic Iron Complexes", *J. Phys. Chem.* **91**, 6198 (1987).
127. R.P. Giugliano and J.J. BelBruno, "Multiphoton Induced Chemistry of Thiirane", *J. Photochem.* **37**, 263 (1987).
128. G.A. Raiche and J.J. BelBruno, "On the Kinetics of the Reaction of Zn (^{1}S) with N_2O", *Chem. Phys. Lett.* **134**, 341 (1987).
129. J.J. BelBruno, (Book Review) *Multiple Photon Infrared Laser Photophysics and Photochemistry*, *J. Am. Chem. Soc.* **108**, 6446 (1986).
130. H.A. Michelsen, R.P. Giugliano and J.J. BelBruno, "Photochemistry and Photophysics of Small Heterocyclic Molecules: I. Multiphoton Ionization and Dissociation of N-Isopropyl Dimethyl Oxaziridine", *J. Phys. Chem.* **89**, 3034 (1985).
131. J.J. BelBruno, "Kinetic Model for Laser-Assisted Reactions", *Chem. Phys. Lett.* **117**, 592 (1985).
132. J.J. BelBruno, J. Gelfand, and H. Rabitz, "Chemical Dynamics in CO-CO and Rare Gas-CO Mixtures", *J. Chem. Phys.* **78**, 3990 (1983).
133. J.J. BelBruno and J. Krenos, "Beam-Scattering Gas Study of the Penning Reaction between Metastable Neon and Carbon Monoxide", *J. Chem. Phys.* **78**, 2800 (1983).
134. J.J. BelBruno, W. Radigan and J. Gelfand, "Self and Helium Broadened Linewidths for the 1-0, 2-0, and 3-0 Bands of Carbon Monoxide", *J. Mol. Spec.* **94**, 336 (1982).

135. J.J. BelBruno, S.D. Augustin, H. Rabitz, and J. Gelfand, "A Rapidly Convergent Expansion Technique for Quantum Mechanical Operators", *J. Chem. Phys.* **76**, 1879 (1982).
136. J.J. BelBruno, J. Gelfand, and H. Rabitz, "Rotational Relaxation Rates in HF and Ar-HF from the Direct Inversion of Pressure Broadened Linewidths", *J. Chem. Phys.* **75**, 4927 (1981).
137. E. Wilczek, J.J. BelBruno, and J. Gelfand, "Voigt Profiles of Spectral Lines: Accuracy as a Function of Peak Transmittance", *App. Spec.* **35**, 443 (1981).
138. A.E. DePristo, J.J. BelBruno, J. Gelfand, and H. Rabitz, "Direct Inversion of High Overtone Collision Broadened Linewidths in the HCl-HCl System: Rotationally Inelastic Rates for Highly Vibrationally Excited Molecules", *J. Chem. Phys.* **74**, 5031 (1981).
139. J.J. BelBruno, M.B. Zughul, J. Gelfand, and H. Rabitz, "Analysis of Collision-Broadened and Overlapped Spectral Lines to Obtain Individual Line Parameters", *J. Mol. Spec.* **87**, 560 (1981).
140. J. BelBruno and J. Krenos, "Population of N_2 $^3\pi$□in Collisions of N_2 with Xenon Metastable Atoms", *Chem. Phys. Lett.* **74**, 430 (1980).
141. J. Krenos and J. BelBruno, "Golden Rule Partitioning of Vibronic Energy: Excitation Transfer by Collisions with Rare-Gas Metastables", in ICPEAC X, edited by M. Barot and J. Theinhardt (Commissoriat a l'Energie Atomique, Paris, 1977).
142. J. Krenos and J. BelBruno, "Golden Rule Partitioning of Vibronic Energy: Excitation Transfer in Collisions of Metastable Argon Atoms with Nitrogen", *Chem. Phys. Lett.* **49**, 447 (1977).
143. J. Krenos and J.J. BelBruno, "Formation of N_2 $^3\pi_u$ and $^3\pi_g$ in Collisions of Metastable Argon with N_2", *J. Chem. Phys.* **65**, 5017 (1976); **66** 5832 (1977).
144. M.A. Brooks, J.J. BelBruno, J.A.D. DeSilva and M.R. Hackman, "A Differential Pulse Polarographic Examination of the 1,4-Benzodiazepines", *Anal. Chim. Acta* **74**, 367 (1975).

Legal Judgment

Establishing Alert Report from FreshAir Sensor as Admissible in Evidence to Establish a Violation of a No-Smoking Policy

Commonwealth of Massachusetts
County of Suffolk Superior Court
Housing Court Department
City of Boston Division
First Justice: Marylou Muirhead
Clerk Magistrate: Robert L. Lewis
Case: 19-CV-2S
Date: January 18, 2019

MVC LLC 40B (Plaintiff, landlord) vs. Lisa Edwards (Defendant, tenant)

> ***"Defendant understands that a FreshAir smoking detector has been installed in her apartment, which defendant agrees accurately and reliably detects smoking in her apartment. In the event that the FreshAir smoking detector sends a report of smoking in the apartment, defendant shall be deemed to be in violation of this agreement and defendant agrees that the alert report from FreshAir shall be admissible in evidence to establish a violation."***

A copy of the original Court Order is attached.

Commonwealth of Massachusetts

SUFFOLK, SS:

HOUSING COURT DEPARTMENT
CITY OF BOSTON DIVISION

MARYLOU MUIRHEAD
FRIST JUSTICE

19 CIV 1251

ROBERT L. LEWIS
CLERK MAGISTRATE

MVC LLC 40B _____ PLAINTIFF(S)

Vs.

Lisa Edwards _____ DEFENDANT(S)

AGREEMENT:

IT IS HEREBY AGREED BETWEEN THE ABOVE NAMED PARTIES THE FOLLOWING:

1) Judgment shall enter for the Plaintiff on all counts.

2) The issuance of an execution and entry of a permanent injunction barring the Defendant from the premises at 40 Berkeley St. Suite 411, Boston, MA shall be stayed on the following terms.

3) In the event Defendant fails to comply with these terms, Plaintiff shall be entitled to relief from the stay provided above upon the filing of a motion for relief which may be heard on 3 days notice.

4) Defendant shall not smoke any cigarettes, marijuana or other products, nor maintain any such items in her apartment at any time. Defendant understands that a "Fresh Air" smoke detector has been installed in her apartment, which Defendant agrees accurately and reliably detects smoking in her apartment. In the event the Fresh Air detector sends a report of smoking in the apartment, Defendant shall be deemed to be in violation of this Agreement and Defendant agrees that the alert report from

THE ABOVE STIPULATION(S) IS AN AGREEMENT WHICH PLACES THE PARTIES UNDER THE RESTRAINT OF A DIRECT ORDER OF THE COURT, THAT THEY DO OR REFRAIN FROM DOING THE PARTICULAR ACTS STATED HEREIN. ANY VIOLATION OF THIS AGREEMENT CAN RESULT IN CONTEMPT, AS THE DOCUMENT IN QUESTION IS INTENDED TO OPERATE AS AN INJUNCTION.

SO ORDERED:
MARYLOU MUIRHEAD, FIRST JUSTICE

_____
ASSOCIATE JUSTICE

_____
DATE: _____

PREPARED BY: _____

_____
Plaintiff

_____
Plaintiff

Lisa Edwards
Defendant

_____
Defendant

Commonwealth of Massachusetts

SUFFOLK, SS:

HOUSING COURT DEPARTMENT
CITY OF BOSTON DIVISION

MARYLOU MUIRHEAD
FRIST JUSTICE

19 CV 1125

ROBERT L. LEWIS
CLERK MAGISTRATE

MVC LLC 40B _____ PLAINTIFF(S)

Vs.

Lisc Edwards _____ DEFENDANT(S)

AGREEMENT:

IT IS HEREBY AGREED BETWEEN THE ABOVE NAMED PARTIES THE FOLLOWING:

Fresh Air shall be admissible in evidence to establish a violation. Defendant shall also not tamper with, disable or interfere in any way with the Fresh Air monitor.

5) Neither the Defendant nor her guests shall cause or create any unreasonable disturbances nor criminal ~~of~~ activity on the property.

6) This agreement shall remain in effect through 1/15/20.

7) All appeals are waived

8) In the event Defendant is transferred to another apartment, the complaint and judgment shall be amended to reflect the new address and this Agreement shall remain in effect.

9) In no event shall any reconciliation or other action of Plaintiff waive this Agreement

THE ABOVE STIPULATION(S) IS AN AGREEMENT WHICH PLACES THE PARTIES UNDER THE RESTRAINT OF A DIRECT ORDER OF THE COURT, THAT THEY DO OR REFRAIN FROM DOING THE PARTICULAR ACTS STATED HEREIN. ANY VIOLATION OF THIS AGREEMENT CAN RESULT IN CONTEMPT, AS THE DOCUMENT IN QUESTION IS INTENDED TO OPERATE AS AN INJUNCTION.

SO ORDERED:
MARYLOU MUIRHEAD, FIRST JUSTICE

ASSOCIATE JUSTICE

DATE: 1/18/19

PREPARED BY: _____

Plaintiff Jeffry Cohn

Plaintiff

Defendant Lisa Edwards

Defendant

Nicotine & Tobacco Research, Volume 15, Number 9 (September 2013) *1511–1518*

ORIGINAL INVESTIGATION

Detection of Secondhand Cigarette Smoke via Nicotine Using Conductive Polymer Films

Yuan Liu BS[1], **Sadik Antwi-Boampong** BS[1], **Joseph J. BelBruno** PhD[1], **Mardi A. Crane** PhD[2], **Susanne E. Tanski** MD[3,4]

[1]*Department of Chemistry, Dartmouth College, Hanover, NH;* [2]*Department of Microbiology and Immunology at Geisel School of Medicine at Dartmouth, Lebanon, NH;* [3]*Department of Pediatrics, Geisel School of Medicine at Dartmouth, Lebanon NH;* [4]*Cancer Control Research Program, Norris Cotton Cancer Center, Geisel School of Medicine at Dartmouth, Lebanon, NH*

Corresponding Author: Joseph J. BelBruno, Department of Chemistry, Dartmouth College, Hanover NH 03755, USA. Telephone: +1-603-646-2270; Fax: +1-603-646-3946; E-mail: jjbchem@dartmouth.edu

Received September 19, 2012; accepted January 8, 2013

ABSTRACT

Introduction: The 2006 U.S. Surgeon General's Report found that there is no safe level of exposure to secondhand smoke (SHS). Many smokers attempt to protect others from exposure to SHS; however, it is difficult to assess effectiveness of these behavior changes. There is a need for personal monitoring devices that provide real-time SHS exposure data; at present, there is no device that measures ambient nicotine levels in real time. The development of such a sensor is the objective of this research.

Methods: A nicotine sensing film comprising the conductive polymer polyaniline was linked with a reporting layer, recording changes in chemiresistance due to adsorption of nicotine. Experiments were carried out in a microprocessor-controlled smoking chamber using sidestream smoke from standard reference cigarettes; up to 10 cigarettes were smoked simultaneously. The exposure chamber was calibrated for total suspended particle, carbon monoxide, and nicotine concentrations.

Results: We found significant *real-time* increases in the resistance of films upon exposure to SHS. The sensors were shown to be sensitive to the number of cigarettes consumed and ambient nicotine and demonstrated reasonable recovery between measurements. The sensors have sufficient sensitivity to detect off-gassing of nicotine or "thirdhand smoke."

Conclusions: A sensing element has been developed that can reliably detect secondhand and thirdhand tobacco smoke in real time through the adsorption of ambient nicotine vapor. The device was calibrated to the number of smoked cigarettes and to nicotine concentration. Development of integrated personal sensors to record exposure to SHS using this technology is currently underway.

INTRODUCTION

There is no safe level of secondhand smoke (SHS) exposure, with SHS causing increased risks of cancer, cardiovascular disease, and childhood illness (U.S. Department of Health and Human Services, 2006). While many smokers believe they are taking sufficient steps to eliminate SHS exposure and harm by smoking away from nonsmokers (e.g., in other rooms, other floors, in front of exhaust fans, out of windows, on balconies/porches), they do not realize that they continue to expose their families. Parents, in particular, desire to protect their vulnerable children; however, there is a lack of accurate measurements of children's exposure. Urine, saliva, or serum cotinine levels are specific to nicotine exposure (tobacco, tobacco smoke, or medicinal nicotine), but there is significant variability in cotinine levels across individuals from similar exposure due to differences in individual metabolism (see review in Avila-Tang et al., 2012). Therefore, a detectable level indicates exposure but is difficult to quantify that exposure with precision, and it is impossible to detect *where or when* that exposure occurred within the preceding several days. In-home room-level testing for tobacco smoke exposure has been conducted using passive or active air sampling procedures; however, the devices involved tend to be costly (e.g., particulate matter pumps with a cost of ~$3000 per unit) or require sending samples to a chemistry lab for assay of tobacco-specific components via gas chromatography and mass spectrometry (Apelberg et al., 2012). Unfortunately, particulate matter detection may also be affected by other sources including cooking with solid fuels, burning candles or incense, or outdoor air pollution (Fernandez et al., 2009; Klepeis, Ott, & Switzer, 2007; Lopez et al., 2012). Monitoring of a tobacco-specific vapor such as nicotine currently suffers from the lack of a real-time measurement (Apelberg et al., 2012); ambient nicotine measurements are typically averaged over a prolonged sampling period of days to weeks given low effective sampling rates (Hammond & Leaderer, 1987). Thus, methods for detecting "how well" a smoker is protecting his/her family are highly problematic.

Previous research efforts have attempted to use feedback on child's cotinine levels as triggers for parental smoking behavior

doi:10.1093/ntr/ntt007
Advance Access publication March 11, 2013

change, with largely disappointing results (Wakefield et al., 2002; Wilson, Farber, Knowles, & Lavori, 2011) excepting modest effects from a study within a population of children with asthma (Wilson et al., 2001). Studies using direct measures of in-home concentrations of ambient nicotine (Emmons et al., 2001) or PM2.5 have shown better success (Wilson, Ritchie, et al., 2013; Wilson, Semple, et al., 2012), suggesting that the specificity of the information regarding smoke exposure from within the home may be more persuasive. The ability to provide real-time feedback in response to specific smoking situations may be even more persuasive to change the behaviors of smokers; however, the possibility of such feedback has previously not been possible given technological limitations. A reliable sensing element is the first step in developing a personal monitoring device for SHS, with the ultimate goal of developing a small, affordable, and wearable device that records cigarette smoke exposure in *real time*, allowing the direct connection of SHS exposure to a smoking event.

Conductive polymers such as polyaniline (PANi) are of great interest as components of electrochemical devices (Lai, Tang, et al., 2011; Lai, Zhang, Li, & Gao, 2011; Zhang, Kong, Wang, Luo, & Kang, 2009) and as agents for a variety of sensing applications (Gopalan, Lee, Ragupathy, Lee, & Lee,. 2009; Srivastava, Kumar, Singh, Singh, & Vijay, 2011; Tran, Nguyen, Nguyen, Do, & Nguyen, 2011). As a sensor for nicotine, the key element of doped, electrically conductive PANi is the presence of protonated nitrogen atoms that give up a proton to nicotine, a base, which is adsorbed to the film from the nascent vapor. Thin film materials can optimize the density and availability of protonated receptor sites, minimize the diffusion distance necessary for the nicotine to travel during binding events, and increase the responsivity of the sensor when the reporting electrode lies beneath the film, as in this research. The various techniques for creating these thin films include electropolymerization (Waltman & Bargon, 1986), spin casting (Psuja, 2007; Yokota, Kitaoka, & Wariishi, 2007), and laser deposition (Chrisey et al., 2003; Frycek et al., 2006). Measurement using conductive polymer films can be performed either by coating the surface of an electrode with the doped polymer and measuring electrical changes with reference to a redox electrode or by making a true planar chemiresistive structure. The latter has advantages, in that it can be used with a variety of conductive polymers, may be designed to create a higher value of resistance, and has the potential for rapid measurements with small, personal-sized devices. In this article, we describe the development of a planar chemiresistive sensor that reports on exposure to SHS from ambient nicotine concentrations in *real time*. This is an important distinction from active or passive time averaging of ambient nicotine or nonspecific PM2.5 measurements, in that it allows for demonstration of changes in air nicotine from a specific smoking event.

METHODS

Materials

Polyaniline (purchased from Polysciences, Inc.) was used as the undoped emeraldine base, with a molecular weight of 15,000 and a conductivity of 10^{-10} S/cm. Formic acid (>98%; purchased from EMD Chemicals) was used to dissolve the polyaniline prior to spin casting and acts as a primary dopant. Secondary doping using 1.0 M aqueous HCl (purchased from Fisher Scientific) increased the sensitivity of the films. For bench laboratory studies, 99% nicotine was used (purchased from Alfa-Aesor). All reagents were used as received without any further treatment. The cigarettes used in the smoking chamber were filtered University of Kentucky 3RF4 reference cigarettes, containing ~0.8 mg of nicotine (Tobacco & Health Research Institute).

Fabrication of Conductive Sensors

The sensing assembly consists of the PANi nicotine–sensing film and an electronic reporting layer. The reporting layer is an electrically conductive electrode patterned into an interdigitated grid with 40 μm fingers and 20 μm spacing, produced on prime grade silicon wafers with a 5000-Å oxide layer. The chromium layer was patterned by photolithography and subsequently wet etched to produce the final electrodes with a total area of 376 mm^2, following vapor deposition of 200 Å of chromium and a 1000 Å overlay of nickel.

Preparation of PANi Solutions and Films

The sensing concept is based on the production of a conductive film that is sensitive to nicotine adsorption, using spin casting of PANi from solution for preparing films. The spin casting solution was produced from formic acid as a 1% (by weight) polymer solution.

An aliquot of 0.5 ml of the PANi polymer solution was dropped onto the silicon reporting layer (described above) and allowed to spread for 20 s. The spin coater was then brought up to 4000 rpm for 30 s. This resulted in deposition of films with a typical thickness of approximately 100 nm. Because the pK_a of formic acid is 3.77 (the amine and imine nitrogen atoms have different pK_a values), PANi in this solution is 50% protonated. To complete the protonation process and increase the sensitivity of the film, secondary protonation in 1.0 M HCl was employed by dip coating for 30 s. After this treatment, background (washed) resistance values were measured, and morphology and roughness were investigated by atomic force microscopy using a Pacific Nanotechnology Nano-1 microscope in close contact mode.

Teague Smoking System/Laboratory Exposure System

Sensors were tested using two different controlled environments with two different goals: a bench laboratory test measured sensitivity to nicotine vapor directly and a smoking machine measurement tested the sensitivity to nicotine from SHS as a function of the number of cigarettes smoked in the machine. In both experimental environments, the change in the resistance of the sensor was measured using a multimeter connected to a laboratory computer.

The laboratory sample system (lab chamber) consisted of a small nylon box, containing spring-mounted electrodes and a small (~3 cm^3) well filled via a syringe through a septum. The sensor assembly was placed on the electrodes above the well and a nylon cap attached using a torque wrench to ensure reproducible pressure of the sensor against the spring-mounted electrodes. Nicotine (1 mL) was injected into the well and the response of the sensor recorded. To follow the recovery of the sensor after exposure to nicotine, dry nitrogen was passed

through the well to evaporate the nicotine. Nicotine was injected at different concentrations and resistance recorded as a function of time at 22 °C. The vapor-phase concentration of nicotine was varied by making liquid mixtures of nicotine in chloroform. Rault's Law provides that the vapor pressure of each component is determined by the mole fraction in the liquid phase. Our polymer sensor is insensitive to chloroform vapor.

The smoking machine experiments were carried out in a Teague Enterprises TE-10 smoking system equipped with two exposure chambers (Teague Enterprises). The TE-10 smoking system incorporates a microprocessor-controlled smoking machine that produces both mainstream and sidestream smoke, or sidestream smoke alone, in conjunction with mixing, aging, and exposure chambers. Smoke is drawn from the combustion chamber into a mixing chamber and then into exposure chambers. Cigarettes are loaded into a wheel, lit, puffed, and ejected; the Federal Trade Commission method of puffing is used, with a 2 s puff, once per minute, smoked for 8 min each. One to 10 cigarettes may be smoked simultaneously. Expended cigarettes are automatically ejected and extinguished in a water bath. Valves control airflow volume during smoke generation and exposure conditions. Valves also permit purging of smoke from within the chambers into dedicated ducting that conducts all smoke outside the building. All measurements using the Teague Enterprises system were made with polymer sensors in an exposure chamber, using calibrated operational parameters for total suspended particle, carbon monoxide, and nicotine concentrations by selected mixing valve settings.

Sensor Response

Measurement of the sensor response to nicotine is accomplished through changes in resistance as a function of time. The resistance, *R,* of the polymer sensor was measured using a Keithley Model 2100 6 ½ Digit Multimeter. During the measurement, constant current of 1 mA was applied and the voltage through the film recorded, providing a resistance value via Ohm's law. Total dissipated power within the sensor was less than 0.5 mW. Sensitivity analysis found that four point measurements were unnecessary, thus all of the reported data were obtained using two contacts. Data were taken at a rate of 1 Hz over as long as 9 hr but typically over considerably shorter times. The background resistance background was measured prior to each exposure (typically 600 Ω); data are reported as normalized resistance, referenced to the initial, out-of-chamber background value.

The films were exposed to a range of analyte concentrations that ensured a challenge to the adsorption process. The results indicate that both the change in the resistance value and the rate of change in the resistance are proportional to the quantity and identity of the analyte adsorbed.

RESULTS

Sensor Morphology

The morphology of the film surface was investigated by atomic force microscopy of films produced on both silicon oxide and glass under the coating conditions described above. The undoped film (prior to treatment with HCl) is rougher than the doped material and more irregular with surface defects. The doped film is smoother, and the minimal occurrence of surface defects provides an ideal material for adsorption of the target nicotine molecule from the vapor phase (data not shown).

Changes in Resistance in Response to Adsorbed Nicotine

Sensor functionality depends upon detecting differences in electrical resistance as a function of the adsorption of nicotine onto the sensor chip. We tested numerous films using pure nicotine in the small lab-built chamber and cigarette exposure as measured in the Teague smoking system. Data and figures presented here are typical of these observations.

Lab Chamber Results

Injection of nicotine into the sample well evoked an immediate rise in the measured resistance. The theoretical values of nicotine concentration were confirmed experimentally by use of a photoionization detector that was sensitive to nicotine but not chloroform. (RAE, 2012) The results of these preliminary studies are shown in Figure 1, where the initial slope upon injection of the sample into the chamber is plotted against nicotine concentration. Figure 1 also includes a typical plot of the signal for pure nicotine vapor as a function of time, postinjection.

The data in Figure 1 provide a calibration of the rate of relative resistance change as a function of parts per billion (ppb) of nicotine in air. The measurements shown were reproducible to within 5%. The data are fit via linear regression with a slope of $1.90 \times 10^{-6}\ \Omega_{rel}\ s^{-1}\ ppb^{-1}$ and a correlation coefficient of 0.99. The slopes are a preferred measure of the concentration; use of absolute resistance changes is problematic since the sensor resistance will continually increase if nicotine remains present in the ambient atmosphere. This calibration is intended for use in reporting sensor data in terms of ppb of nicotine rather than as a function of cigarette exposure.

Teague Smoking Machine Results

Figure 2 presents the entire response curve over time in response to smoking a single cigarette in the Teague system. During the smoking process, sidestream smoke was fed into the exposure chamber and the resistance increased as long as the smoking continued, indicating continued adsorption of nicotine into the film. The signal stopped increasing as the cigarette was extinguished and decreased slowly because air entering into the exposure chamber from the smoking system contained no additional nicotine. After approximately 6 min, the chamber was purged with 100% fresh (room) air and the sensor resistance dropped to a level approximately 20% above the chamber background. The initial slope of the signal was determined to be $8.73 \times 10^{-4}\ \Omega_{rel}\ s^{-1}$, indicating, from our calibration curve in Figure 1, a nicotine level of 450 ppb for this exposure. The system calibration at the inflow/outflow settings of the exposure chamber provides that the dynamic nicotine concentration in this situation from the cigarette smoke alone is 0.5 ppb. Note that the background reading of the sensor (the resistance at the zero time point in the smoking apparatus) immediately increases as the film is placed into the exposure chamber, indicating a background level of nicotine before engaging the smoking apparatus and hence a higher total concentration.

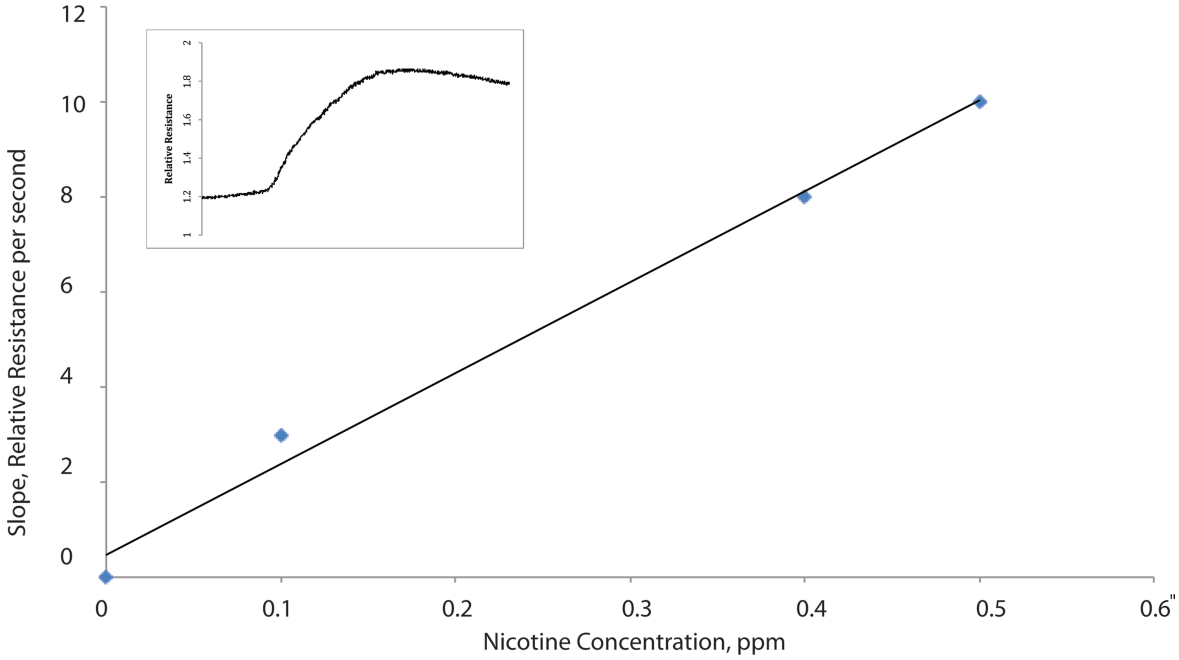

Figure 1. Response of the sensor to vapor-phase nicotine from liquid nicotine at 22 °C. Plot of signal as a function of time for pure nicotine vapor (inset).

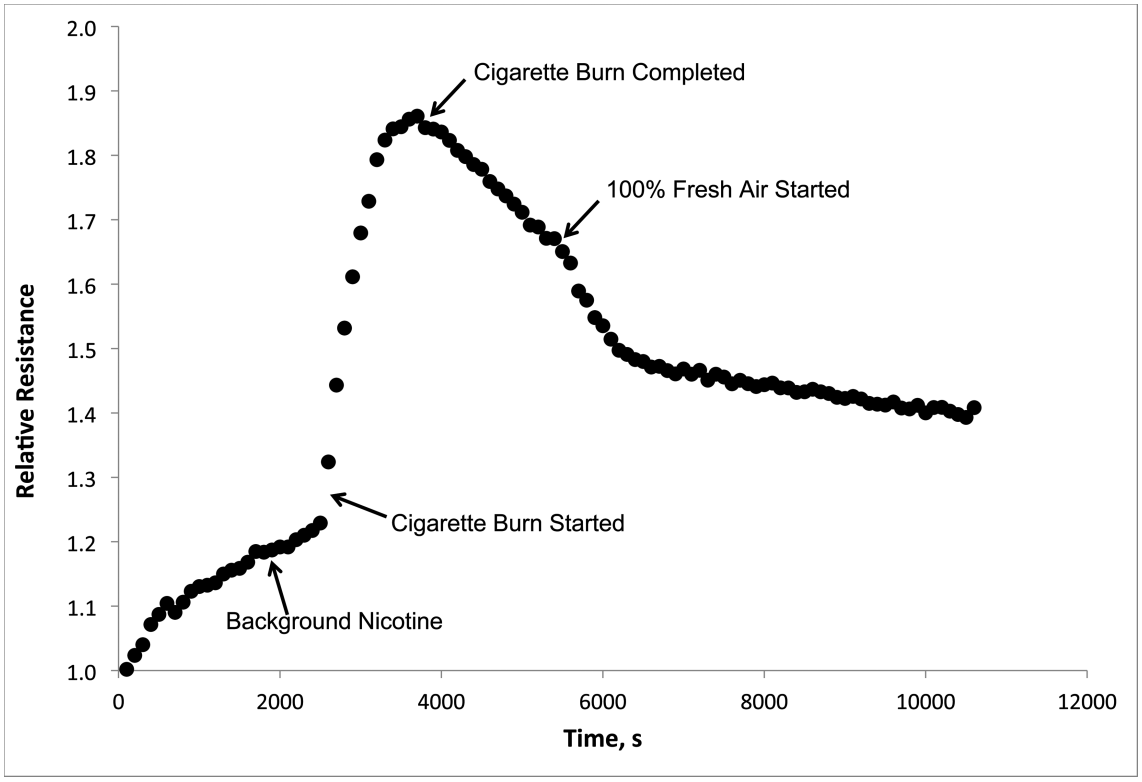

Figure 2. Response of the sensor, in terms of relative resistance, generated from a single cigarette in the Teague system. Note that the sensor detects nicotine adsorbed on the walls in the chamber from previous experiments, so-called thirdhand smoke.

Figure 3 demonstrates a set of sequential exposures in the Teague system, using varied numbers of simultaneously smoked cigarettes, each followed by a brief fresh air blowout. Cigarettes were smoked over a period of 8 min (in a manual lighting mode), during which sidestream smoke was mixed with an equal volume of fresh air and fed into the exposure chamber. Following the extinguishing of the cigarette, fresh air was blown into the exposure chamber for a period of 6 min (purge). The decrease in resistance during the fresh-air phase shows that nicotine is desorbed from the sensor, restoring the resistance to a

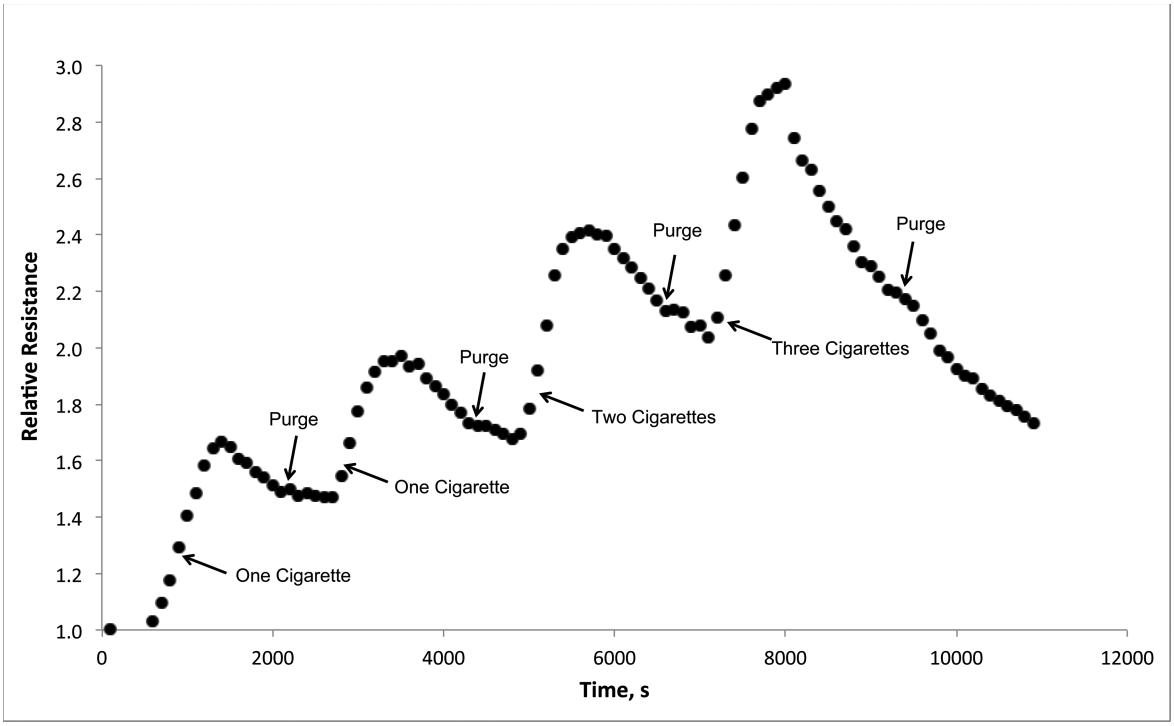

Figure 3. Response of the sensor, in terms of relative resistance, generated from cigarette smoking in the Teague system. The plot shows the response to different numbers of cigarettes smoked simultaneously. Clean, smoke-free air was passed through the chamber between successive experiments.

smaller value. The slopes of the rising signals are also related to the number of cigarettes simultaneously consumed. The system provides nominal dynamic concentrations of 0.75 ppb and 1.11 ppb of nicotine from sidestream smoke generated by two and three cigarettes, respectively. The initial slopes for the three different smoking levels were 9.62×10^{-4} Ω_{rel} s^{-1} (510 ppb), 1.63×10^{-3} Ω_{rel} s^{-1} (1030 ppb), and 1.72×10^{-3} Ω_{rel} s^{-1} (1,100 ppb), respectively, during consumption of one, two, and three cigarettes. Note the agreement between the slopes in Figures 2 and 3 for a single cigarette and the measured increases in nicotine exposure for multiple cigarette exposure. Sensor fatigue caused by the insufficient 'off time' to remove nicotine from the sensor was observed for the final cycle shown in the figure.

Finally, Figure 4 contains the results from several successive runs in which 10 cigarettes (nominally providing 3.16 ppb of nicotine) were simultaneously smoked in order to test the response and recovery in a heavy smoking situation. The sensor background resistance was measured in ambient room air prior to insertion in the exposure chamber. After a 6-min delay (following cigarette extinguishment), a new burn was begun, followed by two additional 10-cigarette exposures. The first 10-cigarette burn resulted in a steep increase with a slope of 1.91×10^{-3} Ω_{rel} s^{-1} (1,000 ppb), less than expected based on the previous figures but reflecting a saturation of easily reached binding sites near the surface of the sensor.

DISCUSSION

This series of experiments demonstrates that a novel sensor based on a polyaniline film can detect ambient nicotine levels in real time, within two different experimental environments, across a wide range of nicotine and sidestream smoke concentrations. This is a leap forward in SHS exposure detection technology as detection of any level of ambient nicotine is specific to tobacco smoke having been present within that space. Previous research has demonstrated that exposure to ambient nicotine is correlated with exposure to the harmful components of tobacco smoke (see Apelberg, 2012 for review). The sensor/chip assembly is particularly innovative, in that it does not require any disassembly of the device or transport to a laboratory for subsequent analysis; the sensor needs only to be linked to a computer to retrieve the data and computationally interpret the normalized relative changes in resistance as nicotine exposure in ppb. This information can then be provided to the end user. Such information could be used to confirm adherence to smoking bans such as in rented motor vehicles, hotel rooms, apartment buildings, restaurants, or bars. Personal use, as noted above, can provide feedback to smokers regarding how well they are achieving true smoke-free environments for their nonsmoking family members.

Notably, as illustrated in each of the smoking system experiments and conspicuously absent in the lab chamber experiments, the background reading of the sensor, or the resistance at the zero time point in the smoking apparatus, immediately increases by 20% as the film is placed into the exposure chamber, indicating a background level of nicotine before engaging the smoking apparatus. Using the experiment illustrated in Figure 2 as an example, prior to our use for the experiment, the smoking chamber had been in constant use for 8 hr and the walls were not cleaned. This suggests that the sensor is capable of measuring nicotine outgassing from the enamel covered metal surface of the chamber's interior walls. This tobacco smoke contamination of rooms and automobiles, or "thirdhand smoke," has been described (Sleiman et al., 2010) and is currently the topic of a new area of research.

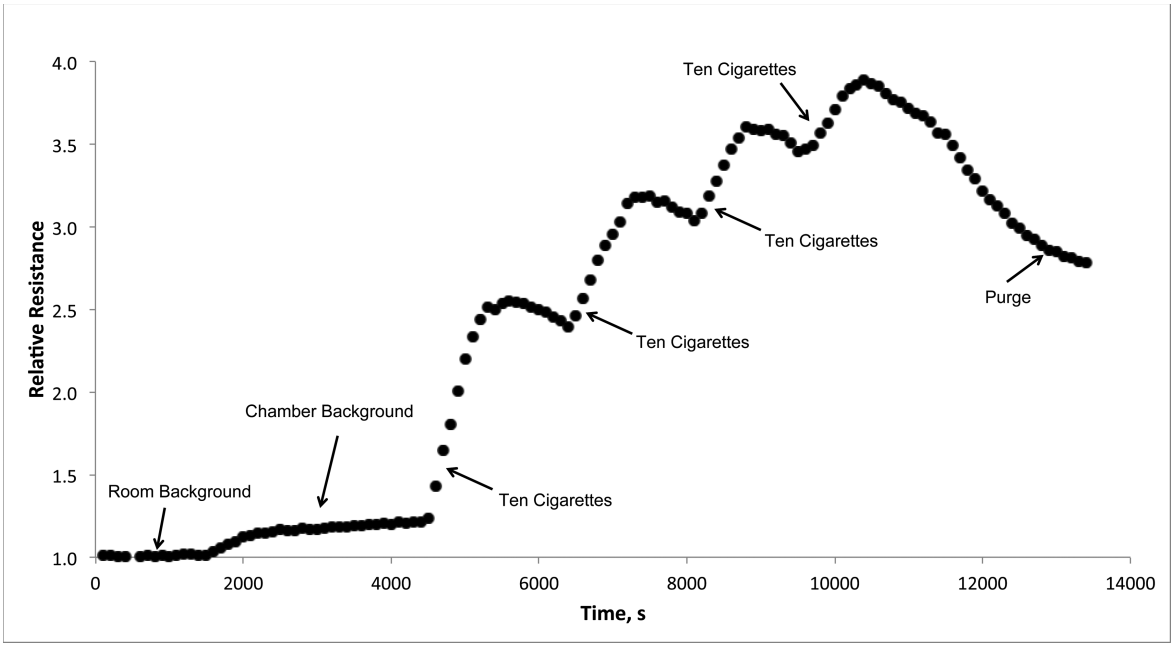

Figure 4. Response of the sensor, in terms of relative resistance, generated from repetitive smoking of 10 cigarettes in the Teague system. The experiment shows that the sensor recovers even in this heavy smoking regime. Note that the sensor again detects nicotine adsorbed on the wall in the chamber from previous experiments.

Limitations

This new technology shows substantial promise for quantification of ambient nicotine, and the same sensor can be repeatedly used; however, the baseline resistance of the sensor does rise with repeated exposures if the sensor is not in a fresh-air environment, allowing nicotine to desorb from the sensor. This can be seen in Figure 3, where the fresh-air phase of the repetitive experiment was not sufficient to bring the sensor back to the original baseline. However, the final exposure cycle shown in Figure 3, with a longer smoke-free period, indicates that a return approximately to the original baseline is possible. Indeed, a resistance measurement made several hours after completing the experiments that are shown in the figure resulted in a value nearly equal to the initial resistance (data not shown). With these repetitive exposures within the smoking chamber, we note simply that the first, single cigarette increases the signal by ~60% and a second consecutive single cigarette furthers the increase by 32%. The next sample, involving two cigarettes, resulted in a 40% signal increase, and the final sample of three cigarettes resulted in a 42% increase in resistance. These differences in resistance measurements with high-intensity exposures are also noted in Figure 4, where the first cigarette burn (of 10 cigarettes) resulted in substantially lower resistance than expected (based on the previous figures), reflecting a saturation of easily reached binding sites near the surface of the sensor. Figure 4 also shows that the absence of significant recovery time following each 10-cigarette exposure decreases the absolute increase in signal (although the third and fourth exposures provide similar increases), with measured changes in resistance of 110%, 25%, 15%, and 9% with these repeated high-intensity exposures. The intention of this particular experiment was to saturate the sensor, exposing it to levels of tobacco smoke that would unlikely be encountered if used as a personal sensing device (given air flow) or even if used as a room-level monitor, given the unlikelihood of such intense exposure within such a small space. The repeated 10-cigarette exposure within the 1 m^3 volume of the smoking chamber would rival that of the smokiest bar with no ventilation at all. Most importantly, this particular experiment indicates that the film is sensitive to its environment, even if the ambient atmosphere has a remarkably heavy concentration of cigarette smoke. The repeated intense exposure/saturation issues will be addressed in subsequent refinement of the device, but may be addressable with computer algorithms to interpret resistance slopes by time.

Impact

The preceding results and discussion primarily focus on changes in the resistance as a function of sensor exposure, but we have ascertained and quantified (Figure 1) the rate of change (slope) of the resistance with both nicotine concentration (in the laboratory chamber) and cigarette exposure (in the smoking system). This dual calibration allows two ways to present exposure data. While in scientific studies one prefers to use nicotine concentrations in ppb, the calibration of detector response to the number of cigarettes consumed in the smoking apparatus provides a useful means of relating SHS exposure to smokers and nonsmokers. Relating SHS exposure of a child (or other nonsmoker) to "the equivalent of xx cigarettes" provides a more striking and readily assimilated message. We hypothesize that such a message would have maximum impact, similar to the ways in which delivering the PM2.5 levels worked in the cited REFRESH study (Wilson, Ritchie, et al., 2013, Wilson, Semple, et al., 2012). We should also be able to correlate our electronic measurements to others currently in use, such as the real-time PM2.5 studies (Semple, Apsley, & MacCalman, 2012), by a cross calibration.

Future

While the size of the polymer films used in the studies depicted above was approximately 1 in.^{2}, the size of the sensing element may be reduced to one-half to one-third without compromising functionality. This allows for smaller and less obtrusive personal sensors. We have explored the application of small, restricted instruction set computer processors to handle data input, storage, and output and are currently refining appropriate candidate electronics. We have developed prototype devices that are powered by a small, long-life (rechargeable) battery that can operate the sensor for several days if data are stored internally and downloaded at the conclusion of a study. The cost of the reusable sensing chip (polymer film plus reporting chip) is currently of the order of USD 30. We found that the polymer may be stripped and recoated for as many as 20 cycles, at which time the chip was still functional and testing halted. Recoating the interdigitated electrodes with fresh polymer for reuse costs pennies for the raw materials. The computer processor is the most expensive aspect of a personal sensor. The current cost of such devices ranges from USD 25–300, depending upon the vendor and required capabilities, which depend on the desired use of the device.

CONCLUSIONS

We have demonstrated that a chemiresistor based on a polyaniline film and interdigitated electrode can provide a *real-time* indication of exposure to secondhand cigarette smoke. The polyaniline film was shown to be sensitive to the number of cigarettes consumed, demonstrated reasonable recovery between exposures, and was functional in the presence of a wide range of exposures to nicotine and tobacco smoke from simulated light-smoking to heavy-smoking environments. The detection of nicotine outgassing or "thirdhand smoke" was also demonstrated to be feasible using the polymer film assembly. These results provide the basis for the development of wearable personal exposure sensors. These exposure sensors can be used to detect personal exposures and to detect nicotine in spaces such as rooms or cars, providing real-time indications of cigarette usage in those environments.

FUNDING

This work was supported by the American Academy of Pediatrics Julius B. Richmond Center of Excellence, funded through the Flight Attendants Medical Research Institute, and by the Norris Cotton Cancer Center at Dartmouth Hitchcock Medical Center.

DECLARATION OF INTERESTS

Dartmouth College has a patent pending for this technology.

REFERENCES

Apelberg, B. J., Hepp, L. M., Avila-Tang, E., Gundel, L., Hammond, S. K., Hovell, M. F., … Breysse, P. N. (2012). Environmental monitoring of secondhand smoke exposure. *Tobacco Control*. Advance online publication. doi:10.1136/tobaccocontrol-2011-050301

Avila-Tang, E., Al-Delaimy, W. K., Ashley, D. L., Benowitz, N., Bernert, J. T., Kim, S., … Hecht, S. S. (2012). Assessing secondhand smoke using biological markers. *Tobacco Control*. Advance online publication. doi:10.1136/tobaccocontrol-2011-050298

Chrisey, D. B., Piqué, A., McGill, R. A., Horwitz, J. S., Ringeisen, B. R., Bubb, D. M., & Wu, P. K. (2003). Laser deposition of polymer and biomaterial films. *Chemical Reviews*, *103*, 553–576. doi:10.1021/cr010428w

Emmons, K. M., Hammond, S. K., Fava, J. L., Velicer, W. F., Evans, J. L., & Monroe, A. D. (2001). A randomized trial to reduce passive smoke exposure in low-income households with young children. *Pediatrics*, *108*, 18–24. doi:10.1542/peds.108.1.18

Fernández, E., Martínez, C., Fu, M., Martínez-Sánchez, J. M., López, M. J., Invernizzi, G., … Nebot, M. (2009). Second-hand smoke exposure in a sample of European hospitals. *European Respiratory Journal*, *34*, 111–116. doi:10.1183/09031936.00180708

Frycek, R., Jelinek, M., Kocourek, T., Fitl, P., Vrnata, M., Myslik, V., & Vroba, M. (2006). Thin organic layers prepared by MAPLE for gas sensor application. *Thin Solid Films*, *495*, 308–311. doi:10.1016/j.tsf.2005.08.178

Gopalan, A. I., Lee, K. P., Ragupathy, D., Lee, S. H., & Lee, J. W. (2009). An electrochemical glucose biosensor exploiting a polyaniline grafted multiwalled carbon nanotube/perfluorosulfonate ionomer-silica nanocomposite. *Biomaterials*, *30*, 5999–6005. doi:10.1016/j.biomaterials.2009.07.047

Hammond, S. K., & Leaderer, B. P. (1987). A diffusion monitor to measure exposure to passive smoking. *Environmental Science & Technology*, *21*, 494–497. doi:10.1021/es00159a012

Klepeis, N. E., Ott, W. R., & Switzer, P. (2007). Real-time measurement of outdoor tobacco smoke particles. *Journal of the Air & Waste Management Association*, *57*, 522–534. doi:10.3155/1047-3289.57.5.522

Lai, B., Tang, X., Li, H., Du, Z., Liu, X., & Zhang, Q. (2011). Power production enhancement with a polyaniline modified anode in microbial fuel cells. *Biosensors & Bioelectronics*, *28*, 373–377. doi:10.1016/j.bios.2011.07.050

Lai, C., Zhang, H. Z., Li, G. R., & Gao, X. P. (2011) Mesoporous polyaniline/TiO_2 microspheres with core-shell structure as anode materials for lithium ion battery. *Journal of Power Sources*, *196*, 4735–4740. doi:10.1016/j.jpowsour.2011.01.077

López, M. J., Fernández, E., Gorini, G., Moshammer, H., Polanska, K., Clancy, L., … Nebot, M. (2012). Exposure to secondhand smoke in terraces and other outdoor areas of hospitality venues in eight European countries. *PLoS One*, *7*, e42130. doi:10.1371/journal.pone.0042130

Psuja, P. (2007). Fabrication of indium tin oxide (ITO) thin films by spin-coating deposition method. In M. J. Ellison (Ed.), *Thin-film coatings for optical applications IV* (p. 667408). *Proceedings of the SPIE*. doi:10.1117/12.735714

RAE Systems, Inc. (2012). MultiRAE Lite. Retrieved from http://www.raesystems.com

Semple, S., Apsley, A., & MacCalman, L. (2012). An inexpensive particle monitor for smoker behaviour modification in homes. *Tobacco Control*. doi:10.1136/tobaccocontrol-2011-050401

Sleiman, M., Gundel, L. A., Pankow, J. F., Jacob, P. 3rd, Singer, B. C., & Destaillats, H. (2010). Formation of carcinogens indoors by surface-mediated reactions of nicotine with nitrous acid, leading to potential thirdhand smoke hazards. *Proceedings of the National Academy of Sciences*, *107*, 6576–6581. doi:10.1073/pnas.0912820107

Srivastava, S., Kumar, S., Singh, V. N., Singh, M., & Vijay, Y. K. (2011). Synthesis and characterization of TiO_2

doped polyaniline composites for hydrogen gas sensing. *International Journal of Hydrogen Energy*, *36*, 6343–6355. doi:10.1016/j.ijhydene.2011.01.141

Tran, L. D., Nguyen, D. T., Nguyen, B. H., Do, Q. P., & Nguyen, H. L. (2011). Development of interdigitated arrays coated with functional polyaniline/MWCNT for electrochemical biodetection: Application for human papilloma virus. *Talanta*, *85*, 1560–1565. doi:10.1016/j.talanta.2011.06.048

U.S. Department of Health and Human Services. (2006). *The Health Consequences of Involuntary Exposure to Tobacco Smoke: A Report of the Surgeon General*. Rockville, MD: U.S. Department of Health and Human Services, Public Health Service, Office of the Surgeon General.

Wakefield, M., Banham, D., McCaul, K., Martin, J., Ruffin, R., Badcock, N., & Roberts, L. (2002). Effect of feedback regarding urinary cotinine and brief tailored advice on home smoking restrictions among low-income parents of children with asthma: A controlled trial. *Preventive Medicine*, *34*, 58–65. doi:10.1006/pmed.2001.0953

Waltman, R. J., & Bargon, J. (1986). Electrically conducting polymers - a review of the electropolymerization reaction, of the effects of chemical-structure on polymer film properties, and of applications towards technology. *Canadian Journal of Chemistry*, *64*, 76–95. doi:10.1139/v86-015

Wilson, S. R., Farber, H. J., Knowles, S. B., & Lavori, P. W. (2011). A randomized trial of parental behavioral counseling and cotinine feedback for lowering environmental tobacco smoke exposure in children with asthma: Results of the LETS Manage Asthma trial. *Chest*, *139*, 581–590.

Wilson, I. S., Ritchie, D., Amos, A., Shaw, A., O'Donnell, R., Mills, L. M., . . . Turner, S. W. (2013). 'I'm not doing this for me': Mothers' accounts of creating smoke-free homes. *Health Education Research, 28*(1), 165–178. doi:10.1093/her/cys082

Wilson, I., Semple, S., Mills, L. M., Ritchie, D., Shaw, A., O'Donnell, R., … Amos, A. (2012). REFRESH—Reducing families exposure to secondhand smoke in the home: A feasibility study. *Tobacco Control*. doi:10.1136/tobaccocontrol-2011-050212

Wilson, S. R., Yamada, E. G., Sudhakar, R., Roberto, L., Mannino, D., Mejia, C., & Huss, N. (2001). A controlled trial of an environmental tobacco smoke reduction intervention in low-income children with asthma. *Chest*, *120*, 1709–1722.

Yokota, S., Kitaoka, T., & Wariishi, H. (2007). Surface morphology of cellulose films prepared by spin coating on silicon oxide substrates pretreated with cationic polyelectrolyte. *Applied Surface Science*, *253*, 4208–4214. doi:10.1016/j.apsusc.2006.09.037

Zhang, J., Kong, L. B., Wang, B., Luo, Y. C., & Kang, L. (2009). In-situ electrochemical polymerization of multi-walled carbon nanotube/polyaniline composite films for electrochemical super capacitors. *Synthetic Metals*, *159*, 260–266. doi:10.1016/j.synthmet.2008.09.018

Characterization of Functional States in Nicotine- and Cotinine-Imprinted Poly(4-vinylphenol) Films by Nanoindentation

Asta Richter,[1] Joseph J. BelBruno[2]

[1]*Department of Engineering, Technical University of Applied Sciences Wildau, 15745 Wildau, Germany*
[2]*Department of Chemistry, Dartmouth College, Hanover, New Hampshire 03755*

Received 12 April 2011; accepted 17 July 2011
DOI 10.1002/app.35270
Published online 3 November 2011 in Wiley Online Library (wileyonlinelibrary.com).

ABSTRACT: Thin, imprinted poly(4-vinylphenol) (PVP) films were produced by spin coating using nicotine or its metabolite, cotinine, as template molecules. The template molecules were extracted from these films and later reloaded (or cross-loaded) from solution. Depth sensing nanoindentation was applied to measure the nanomechanical properties of the imprinted polymer films. Changes in the nanomechanical properties were correlated to the functional state of the imprinted polymer, allowing identification of the films in their "as produced" state, "template removed state or "reloaded" state. In addition, the nanomechanical properties were capable of identifying which of the two template molecules were inserted in to a film. Reinsertion of a template molecule into a "template removed" film was found to increase the nanohardness over the values recorded for the "as produced" film. This behavior was discussed in terms of the hydrogen bonding characteristics of the materials (through density functional calculations) and the physical properties of poly(4-vinylphenol) coatings. © 2011 Wiley Periodicals, Inc. J Appl Polym Sci 124: 2798–2806, 2012

Key words: molecularly imprinted polymer; nanoindentation; nanohardness; density functional theory (DFT) calculations

INTRODUCTION

Molecular imprinting is a technique that allows for the production of molecule specific receptors that are analogous to biological receptor binding sites without the cost or environmental sensitivity of the natural systems.[1–5] Molecularly imprinted polymers (MIPs) may be based on either covalent or noncovalent binding between the host polymer and the target or template molecule. The wet phase inversion procedure[6–9] for preparation of MIPs involves a polymerized starting material that is dissolved with the template in a theta solvent. A template-host network is allowed to form in solution and precipitated by immersion in a nonsolvent. Originally developed to produce MIP membranes, we have adapted this procedure to the production of thin, 300 nm to 5 μm, films via spin coating[10–12] and hydrogen bond interactions between the template and host polymer.

Nicotine is a characteristic component of tobacco smoke, and cotinine is a major metabolite of nicotine that is detected in the urine of smokers. Other reports of nicotine MIPs have appeared in the literature. For example, a nicotine-targeted MIP based on the synthesis of the polymer from methacrylic acid monomers has been previously reported.[13] In this report, we describe the production of a poly(4-vinylphenol) (PVP)-based MIP film produced by combining the phase inversion process with spin coating. We have previously reported[14,15] on the use of depth sensing nanoindentation[16–23] to study the nanomechanical properties of MIP films. We have reported the nanohardness and elastic modulus to be dependent upon the functional state of the MIP. That is, whether the MIP is in an "as-produced" state, has had the template molecule removed or has had the template (or a related molecule) reinserted into the emptied MIP. In this report, we describe these nanomechanical measurements for the nicotine- and cotinine-containing MIPs and provide a rationale for the observed changes in these measurements with changing functional state.

Additional Supporting Information may be found in the online version of this article.

Correspondence to: J. J. BelBruno (jjbchem@dartmouth.edu).

Contract grant sponsor: Harris German-Dartmouth Distinguished Visiting Professorship (Dartmouth College).

EXPERIMENTAL

Production of MIP films

Poly(4-vinylphenol) is a less commonly used polymer, but its aromatic nature and hydrogen bonding potential make PVP an ideal host matrix for MIPs.

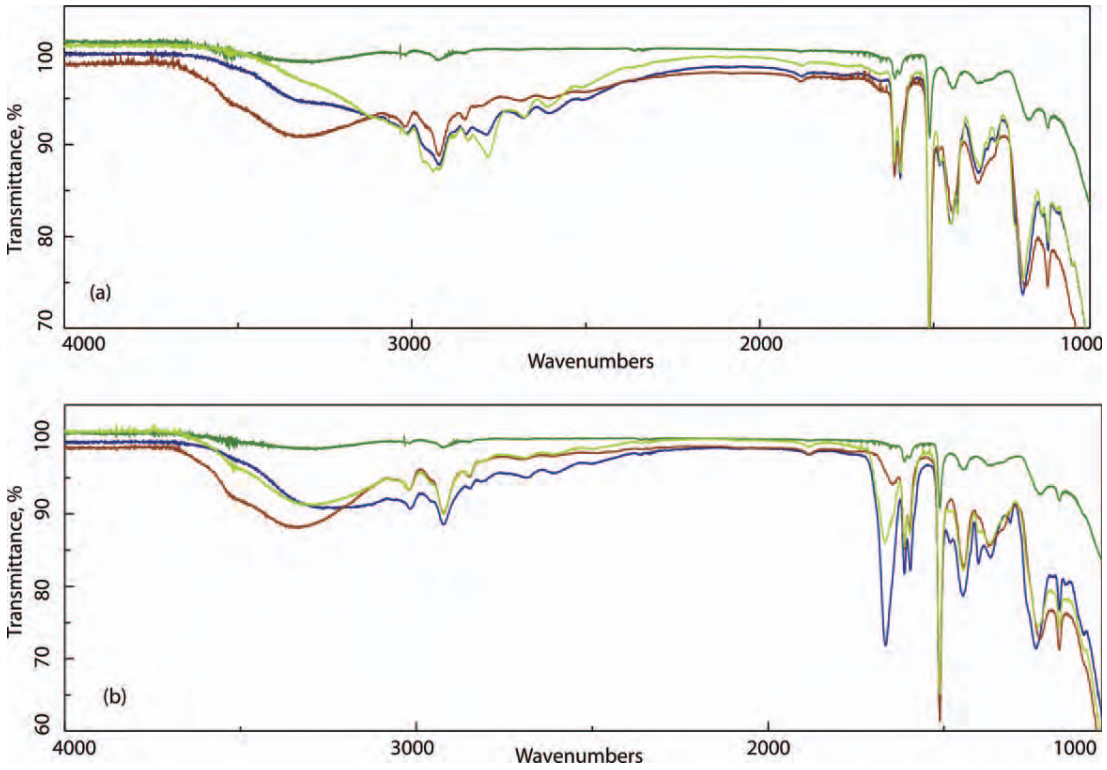

Figure 1 Control (dark green), as produced MIP (blue), template extracted MIP (red) and template reinserted MIP (light green) infrared spectra for (a) nicotine and (b) cotinine templated films. [Color figure can be viewed in the online issue, which is available at wileyonlinelibrary.com.]

The PVP films are produced by spin coating; a simple deposition technique that is sensitive to the composition and viscosity of the solution and the rotating speed of the plate.[24]

Solutions composed of 10 mL of methanol (Acros Organics; ACS Reagent Grade 99.8%) with 10 wt % of PVP powder obtained from Polysciences, Inc. (MW = 22,000; T_g 150°C) and 5 wt % of nicotine (Sigma-Aldrich; PESTANAL® Analytical Standard) or cotinine (Sigma; ~ 98%) were nitrogen purged, covered, and stirred at room temperature for 24 h. Control films (NIPs) were similarly produced but without the nicotine or cotinine. This procedure differs from the conventional MIP production process and is related to the so-called phase inversion production method. It is a preferred process for film production, as MIPs produced by the conventional process would still require later dissolution before casting. Films were spin cast from these solutions onto 22-mm-square glass microscope cover slips. Typically, the slides are cleaned in nitric acid and then prewashed on the spin coater with spectroscopic grade isopropanol and acetone before polymer deposition. The coating solution was dropped onto a stationary substrate, and the spin coater was operated at 4000 rpm for 30 s with negligible ramp up time. The rotation spreads the solution evenly over the surface and also causes the solvent to evaporate leaving a thin film of solid material on the substrate. The concentration of PVP in the casting solution is the dominant variable for the film thickness, which increases rapidly with increasing concentration (solution viscosity), as shown in previous reports.[10] We have not completed a comprehensive study of film thickness as a function of these parameters but have measured the thickness of films made under the conditions cited here to be typically near 1 μm. Cast films are quite stable and may be stored for an indefinite time.

The template molecule was removed from the film by immersion in deionized water for 5 h. Nicotine (or cotinine) removal was confirmed by FTIR measurements. Template reinsertion (or reinsertion of the complementary template molecule) was accomplished by immersion of the template extracted (or control) film in a 5 wt % solution of the template molecule in deionized water for 2.5 h. This reinsertion, as with the template removal procedure, is an equilibrium-controlled process and reinsertion occurs to ~ 50% of the initial concentration (via qualitative FTIR measurements). Additional immersion time was not found to increase the relative amount of template molecule reinserted into the film. FTIR spectra were recorded at 1 cm^{-1} resolution over the energy range from 4000 to 1000 cm^{-1}. Typical spectra are shown in Figure 1 for both

templates. In terms of qualitative indications of template presence, the band between $\sim$ 3400 and 2900 cm^{-1} for the —OH stretch of PVP broadens, and some of the weak discrete transitions grow in when hydrogen bonded to nicotine or cotinine. In addition, at $\sim$ 1700 cm^{-1}, the presence of the carbonyl band of cotinine confirms the interaction of that template with the polymer in the film. The presence of either template will result in the observation of a weak carbon–carbon band at $\sim$ 1500 cm^{-1}. The surface topography of the films is characterized by average roughness measurements, R_a, using scanning force microscopy (SFM). It is defined as the average deviation of the profile from a mean line or the average distance from the profile to the mean line over the length of the assessment. The surface roughness, R_a, is given by the sum of the absolute values of all the areas above and below the mean line divided by the sampling length.

Nanoindentation measurements

All nanoindentation experiments were performed using the electrostatic transducer of the Hysitron triboscope in the UBI 1 as described in a previous publication.[25] Briefly, the data consist of a load-displacement curve. For soft samples such as polymers, the stiffness of the internal springs holding the indenter must be subtracted from the applied load to obtain the sample stiffness. Hardness, H, is calculated in the now standard format,[17] as the applied load, F, divided by the area, A_c, of the indenter tip at the contact depth, h_c; the area is depth dependent. The modulus is derived from the slope of the load-displacement curve upon unloading when the sample elastically recovers. Investigations are performed with a blunted 90° diamond cube corner tip. The calibration of the tip to determine the depth dependent area function $A_c(h_c)$ was obtained with the standard curve-fitting method using fused quartz with its known reduced modulus as the reference material. Additionally, calibration with a sharp silicon grating was performed.[26] Thermal drift is measured and the effect is compensated in the resulting data. Typical drift rates range up to 0.5 nm/s. The penetration depth of the indent should not exceed 30% of the polymer film thickness to avoid substrate effects. Our experiments have been performed with penetration depths less than 30% of the total thickness.

If loading and unloading are repeatedly performed at the same location on the sample surface, depth dependent mechanical properties are obtained.[15,18,21] Eight cycles of multi-indentation have been performed to calculate the depth dependent hardness and the indentation modulus, as shown in Figure 2. As described in previous reports,[25] multicycling means, after loading to a maximum load, F_{max}, the sample is partially unloaded to a minimum load, $F_{min} = 0.1$ to 0.25 F_{max}, required to prevent the tip from losing contact with the sample and sliding to a new lateral position. The sample is then reloaded to the same or an increased maximum load ($F_{max} + \Delta F$) and the cycle is repeated. Multicycling delivers a set of data that includes the entire material response. Average values are obtained from several measurements at different locations on the same sample set.

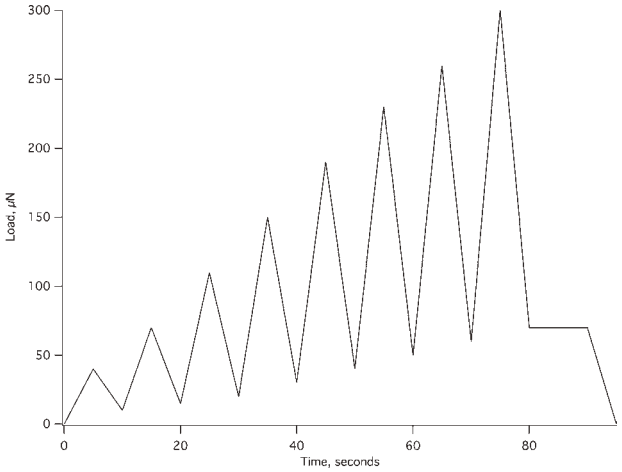

Figure 2 Load-time function for multi-indents with eight cycles as used in this study.

COMPUTATIONAL DETAILS

All optimizations were performed with NWChem, a Computational Chemistry Package for Parallel Computers, v5.1,[27] with no symmetry or geometric constraints. The correlation and exchange effects were calculated using the Perdew-Burke-Ernzerhof (PBE) exchange-correlation functional[28] with the 6-31G* basis set[29] for all atoms. Several initial orientations of the PVP molecule(s) relative to nicotine or cotinine were optimized to ensure that the total energy of the complex was not dependent upon this factor. All calculations were run in parallel on a Linux cluster comprised of 94 Quad-Core (2x) AMD Opteron nodes (752 cpus) and 6 Quad-Core (2x) Intel nodes (48 cpus). In aggregate, the Linux cluster has 3 terabytes of memory and more than 35 terabytes of disk space. Geometric structures were visualized using Avogadro.[30]

RESULTS AND DISCUSSION

Control PVP and MIP film general features

The structure of the MIP and NIP films depends upon several factors. These include temperature and spin casting conditions such as speed and deposition

TABLE I
Measured Surface Roughness Over a 130 × 130 μm Nicotine Film Sample

Functional state[a]	R_a (nm)
NIP	11.5
As produced	69.2
Template removed	44.1
Template reinserted	33.1

[a] Functional state definition: PVP-X indicates an "as produced" MIP where N = nicotine and C = cotinine); PVP-X-Y indicates a MIP imprinted with X, which is subsequently removed and Y is inserted from solution.

time, and the PVP concentration of the solution. Measured values for surface roughness, R_a, for a 130 μm square measurement area of nicotine films are presented in Table I. The pure PVP films deposited from the casting solution containing 10% polymer have a characteristically smooth morphology. In the investigations presented in this article, the pure PVP NIP film has a surface roughness of 11.5 nm. No significant morphological features are found in the control PVP films; i.e., the films are flat. The "as produced" MIP films containing nicotine template molecules show a different surface morphology in comparison to the control films. Surface stripes, representing different heights, are the main surface feature. The surface roughness of this type of sample was measured to be 69.2 nm. SFM images on the stripes as shown in Figure 3(a) represent flat areas with a nanosize ripple structure. Removal of the nicotine from the MIP results in a loss of the stripe morphology and the observation of a number of pores in the surface, Figure 3(b). The pores are apparently formed during the solidification process of the polymer films and are caused by the presence of the template molecules and the porogen solvent during the film growth process.[12] The assumption is that the pores are present in the "as produced" samples but lie beneath the stripe morphology. The template molecules are smaller than the size of the pores observed in our films. The additional volume of the measured pores results in part from the geometrical form of the template molecule, the arrangement of that molecule within the polymer host, and the evaporation of the solvent through the solidifying polymer film. Pores are a desirable property for the MIPs; they allow for more contact between an analyte solution and molecular cavities within the bulk of the film. The surface roughness of the nicotine-removed MIP is 44.1 nm. Reinsertion of nicotine into this MIP partially restores the strip morphology but has minimal effect on the roughness of the surface (R_a = 33.1). The different film morphology in the SFM images is characteristic for the presence or absence of the template molecules.

Nanomechanical properties

The elastic behavior of pure PVP films occurs by deformation of the polymer molecules and movement of the chains after the adhesion energy has been overcome. Contact pressure (hardness) will vary even for homogeneous matter such as the control sample, as the deformation starts with purely elastic deformation, and after yielding, the plastic contributions increase. Multicycling also allows to study visco-elasto-plastic properties of the polymer.[15]

Typical multicycling load-displacement curves for MIP films with nicotine and cotinine template molecules in the casting solution for the spin coating process are shown in Figure 4. From the load-displacement curves in Figure 4(a), it is clear that the "as produced" nicotine-loaded MIP films, PVP-N for

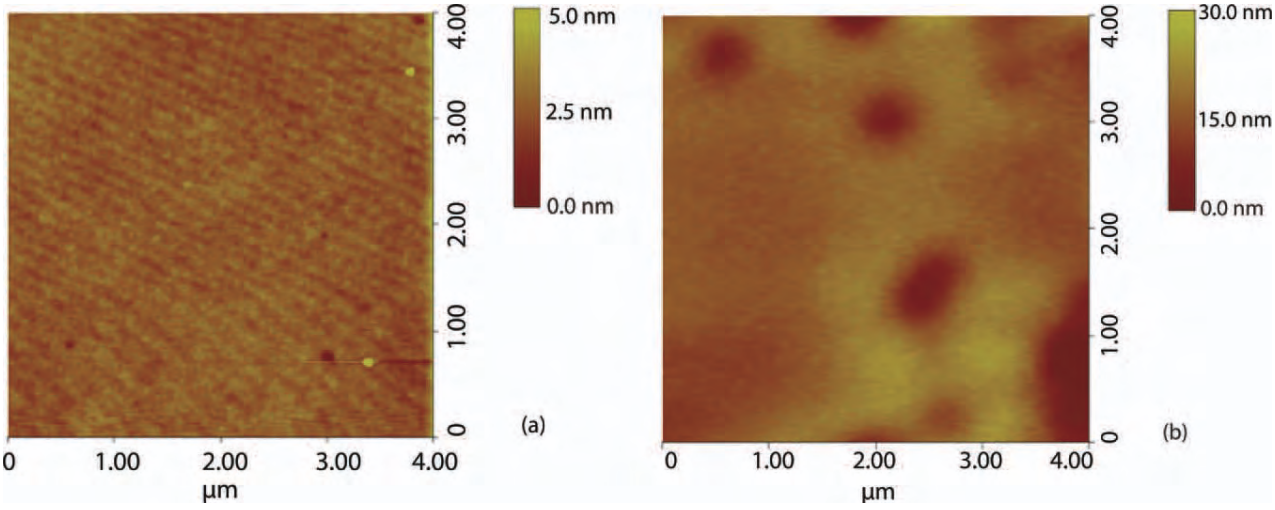

Figure 3 SFM images of size 4 × 4 μm of (a) an "as produced" nicotine imprinted film and (b) a "nicotine removed" imprinted film. [Color figure can be viewed in the online issue, which is available at wileyonlinelibrary.com.]

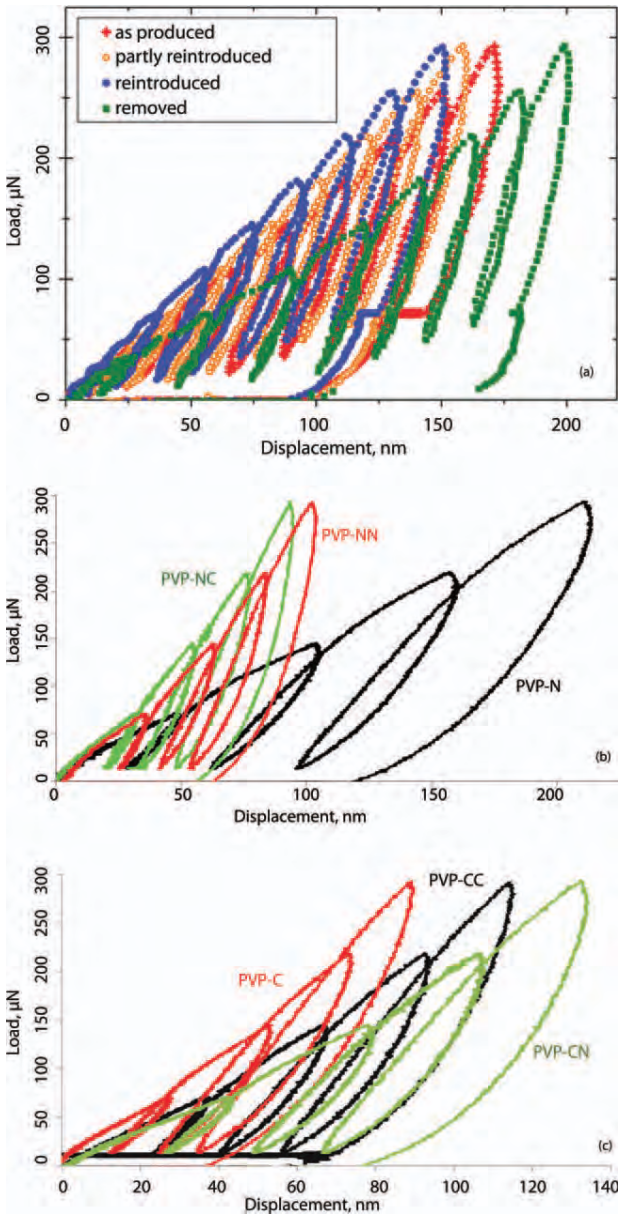

Figure 4 Load-displacement curves (a) as average values for nicotine imprinted PVP samples and specific examples of reloading with the original or alternative template in (b) nicotine-based PVP-N and (c) cotinine-based PVP-C. PVP-X indicates an as produced MIP: N = nicotine and C = cotinine); PVP-X-Y indicates a MIP imprinted with X, which is subsequently removed and Y is inserted from solution. [Color figure can be viewed in the online issue, which is available at wileyonlinelibrary.com.]

example, have average indentation depths of ~ 175 nm with a maximum applied load of 300 μN; removal of the nicotine increases the penetration depth to nearly 200 nm. Surprisingly, reinsertion of nicotine reduces the penetration depth to a value 35 nm less than that of the original imprinted film. Clearly, the reintroduced presence of the template molecule in the MIP leads to a stiffer film. Analogous results are obtained for the cotinine-imprinted films. The assignment of the basis of the change in nanomechanical properties to the template is reinforced by the fact that a MIP with the template removed is less stiff than a pure PVP film for the same applied load. The process of reloading nicotine-based PVP-N and cotinine-based PVP-C with the same or the alternate template molecule is investigated in more detail and results are shown in Figure 4(b,c) using a four-cycle multi-indentation function. Reloading of the molecule that was not the original template alters the mechanical properties of the functional state. The results indicated that the slightly larger cotinine molecule could be inserted in the PVP-N system and an increase of hardness and reduced modulus in comparison to the as produced PVP-N state and nicotine reloaded PVP-*N*-N functional state was observed. This is reflected in the load-displacement curves in Figure 4(b). On the other hand, the reloading of the smaller nicotine molecule into the PVP-C system created a softer material, Figure 4(c), as the molecular pore is not completely filled and the hydrogen bonding to the polymer is altered. The result is that the PVP-C-N functional state has a lower hardness and a lower reduced modulus than that of the as produced PVP-C functional state or that of the nicotine reloaded PVP-*N*-N film. However, these values are still larger than those for the as produced nicotine imprinted PVP-N film.

The nanomechanical behavior of the polymer films is summarized graphically in Figure 5 and Table II with the average values of the depth dependent hardness and indentation modulus and their standard deviation. Hardness and indentation modulus values are fairly constant with indentation depth. At larger depth, a slight increase in both values is noticeable, which indicates contributions from the harder glass substrate. The hardness of the control PVP film has a value of 0.38 GPa with an indentation modulus of 11.7 GPa. MIP films with cotinine, PVP-C, are stiffer with a hardness value of 0.59 GPa and an indentation modulus of 14.7 GPa. Nicotine-imprinted films, PVP-N, are slightly stiffer than the control film with a hardness value of 0.43 GPa and a modulus of 11.6 GPa. Extraction of the template molecules leaves the molecular cavities present in the polymer matrix, but the space they once occupied is empty. Thus, the network character and, therefore, the mechanical properties change; see the load-displacement curves in Figure 4(a). For example, the hardness for MIP films with nicotine extracted yields a smaller value of 0.31 GPa for the hardness. Reloading nicotine into a nicotine-imprinted film from which the template has been removed or cotinine into an extracted cotinine-imprinted film results in a film with greater nanohardness than the original as produced film. The percentage increase in hardness is greater for the

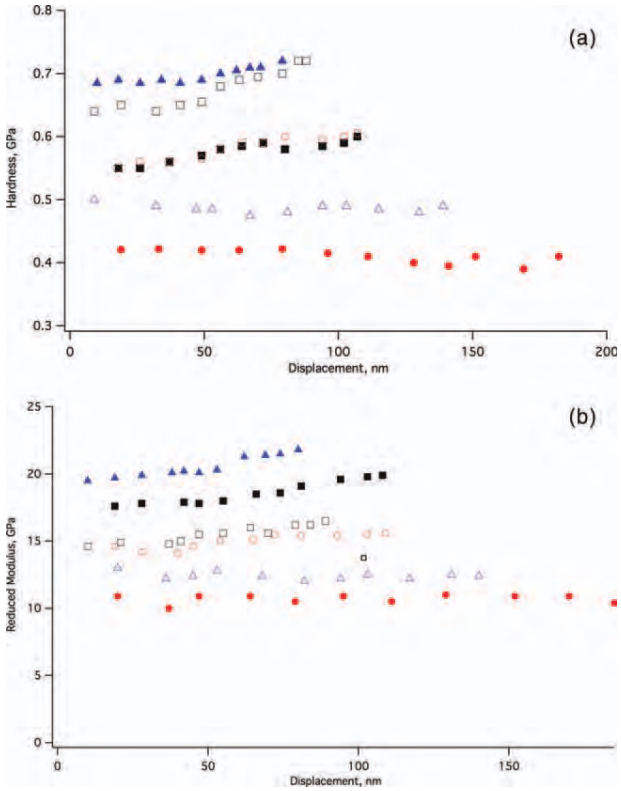

Figure 5 Depth-dependent hardness and reduced elastic modulus results for various functional states of the imprinted polymers. PVP-X indicates an "as produced" MIP N = nicotine and C = cotinine); PVP-X-Y indicates a MIP imprinted with X, which is subsequently removed and Y is inserted from solution. Legend: ●, PVP-N; ■, PVP-NN; ▲, PVP-NC and ○, PVP-C; □, PVP-CC; △, PVP-CN. [Color figure can be viewed in the online issue, which is available at wileyonlinelibrary.com.]

reinsertion of nicotine into a nicotine-targeted MIP than for cotinine into a cotinine-targeted MIP. In addition, cross reloading, that is nicotine in to an extracted cotinine-imprinted film or vice versa, measured hardness is greater than that of an as produced film for the reloading component. Loading, extraction and reloading of nicotine or cotinine in the MIP films are clearly measurable with the nanoindentation technique. Therefore, the different functional states can be distinguished by nanoindentation.

These results support the model of a strongly hydrogen-bonded network among the polymer chains via template molecular linkers. In the ideal case, a molecular cavity with a nicotine template molecule is formed with two hydrogen bonds that crosslink two PVP molecules; cotinine has three such potential hydrogen bonding sites. However, the imprinting process can be incomplete with fewer than the maximum number of hydrogen bonds established. Template molecules can bond to the polymer molecule at several points along the chain with efficiencies dependent upon the number and distribution of template molecules in the MIP film. From the nanomechanical investigations, it is suggested that hydrogen bonding of the template molecules between the PVP chains: (1) results in a crosslinking between the chains, (2) separates the PVP molecules (preventing an easy movement of the chains), and (3) reduces the adhesion energy between pure PVP molecules. This may result in both mechanically stiffer and softer MIP networks. We suggest two different molecular mechanisms for the polymer response during an applied external contact pressure. In pure PVP, the indentation tip can cause a deformation of the PVP molecules and a sliding motion between the chains. The molecular cavities and micropores change the mechanical properties in two directions compared to pure polymer films. Filled cavities (template loaded MIP) show an increase in hardness in comparison to pure PVP films. This implies that a stiffer molecular network is established. In MIP films, the chains are fixed by hydrogen bonds and the sliding motion is inhibited in general. The filled molecular cavities prevent strong elastic deformation. Empty cavities, after extraction of the template, result in a decrease in the hardness. This could be attributed to the empty MIP network more easily squeezed together (the empty cavities act as structural defects), resulting in a lower hardness in comparison to the pure polymer network. In MIP films, the PVP chains are fixed by the hydrogen bonds and the formed molecular cavities, but the deformation around the empty cavities is flexible (breathing cavities). Therefore, no gliding motion of the chains occurs. This means, the main effect for the change of the mechanical properties in different stages of MIP films originates from the formed molecular cavities. If they are filled with the template molecule the material is harder; if the cavities are empty, the compression of the cavities leads to a much softer material. The elastic compression of the empty cavities and pores acts in the same

TABLE II
Hardness and Elastic Modulus Values for Nicotine- and Cotinine-Imprinted PVPs

Template/Functional State[a]	*H* (GPa)	*E* (GPa)
PVP-N	0.41 ± 0.03	11.1 ± 1.89
PVP-N-N	0.58 ± 0.04	18.9 ± 2.9
PVP-N-C	0.7 ± 0.03	20.0 ± 2.1
PVP-C	0.59 ± 0.03	14.7 ± 1.2
PVP-C-C	0.69 ± 0.04	15.7 ± 1.2
PVP-C-N	0.48 ± 0.01	12.6 ± 0.6

[a] Functional state definition: PVP-X indicates an "as produced" MIP where N = nicotine and C = cotinine); PVP-X-Y indicates a MIP imprinted with X, which is subsequently removed and Y is inserted from solution.

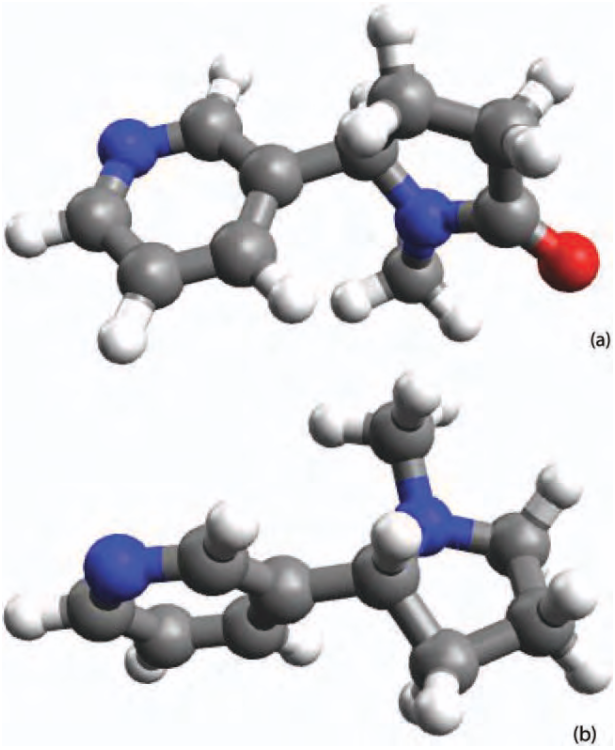

Figure 6 Optimized structures for the cotinine (a) and nicotine (b) imprint molecules. [Color figure can be viewed in the online issue, which is available at wileyonlinelibrary.com.]

direction as the mechanism of deformation and gliding of the PVP chains.

Computational study of hydrogen bonding

Reports in the literature indicate the usefulness of computational chemistry in selecting a polymer host for MIP development with a particular target molecule.[31] However, computational studies may also be useful in providing information to understand experimental MIP results, the task to which we have applied DFT here. The optimized structures of nicotine and cotinine were first obtained for reference and are shown in Figure 6 with the coordinates provided in Supporting Information Table I. These molecules differ only by the addition of a carboxyl group on the pyrrolidine ring of cotinine. The geometry of the planar pyridine ring, including bond lengths, in the two molecules is identical and they differ little in overall size, leading to some expectation that it would be possible to cross-load MIPs templated for one or the other of these related molecules. The presence of the oxygen atom in cotinine results in bond shortening in the pyrrolidine ring, as well as a further distortion from planarity relative to the nicotine pyrrolidine ring. The pyrrolidine nitrogen becomes more sp^2-like rather than the pyramidal angle observed in the nicotine molecule. As a final reference point, the 4-vinylphenol (4VP) dimer structure was optimized and was found to have a hydrogen bond length of 1.876 Å and a hydrogen bond energy of 0.34 eV. The geometric parameters of the monomeric 4-vinylphenol molecule are unchanged in the dimer.

Nicotine has two potential hydrogen binding sites and cotinine has three such sites. The optimized structures for the interaction of nicotine with two monomers and cotinine with three are shown in Figure 7. In both clusters, the optimized 4-vinylphenol geometry is identical to that of the unbonded

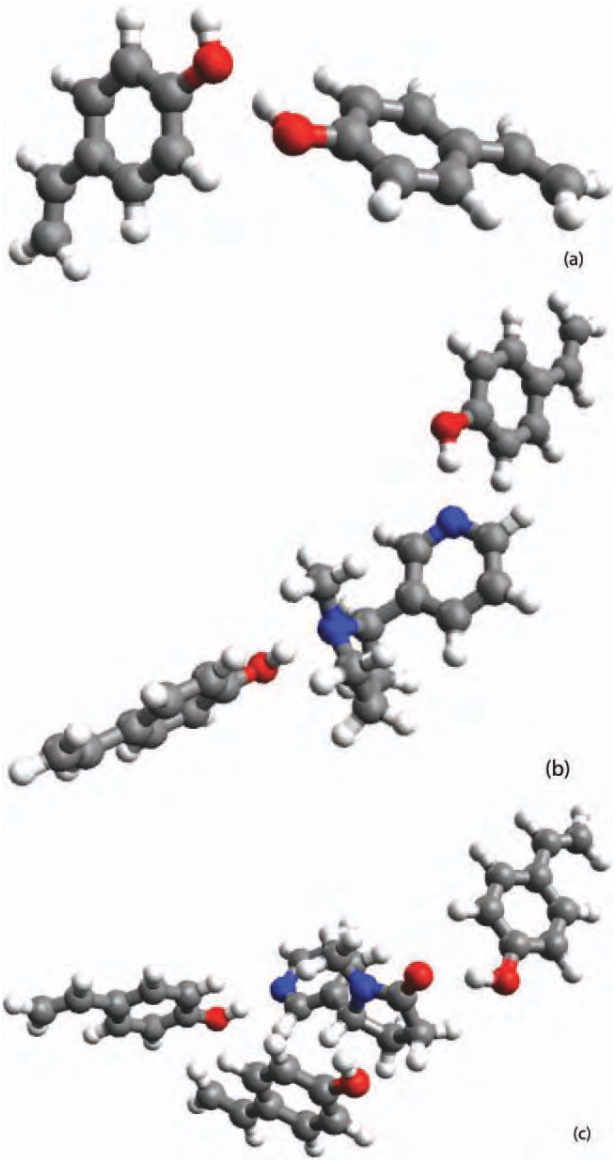

Figure 7 Optimized hydrogen bonded structures for (a) a 4VP dimer, (b) a nicotine plus two 4VP molecular cluster, and (c) a cotinine plus three 4VP molecular cluster. [Color figure can be viewed in the online issue, which is available at wileyonlinelibrary.com.]

molecule and the pyridine ring bond lengths are unaffected by the hydrogen bond. The hydrogen bond from 4VP to the pyridine nitrogen in nicotine has a length of 1.822 Å, whereas that to the pyrrolidine nitrogen is 1.788 Å. The C—N bond lengths in this ring both increase. The total hydrogen bonding energy is 0.84 eV. In cotinine, only two hydrogen bonds form. The bond to the pyridine nitrogen has a length of 1.820 Å and that to the carboxyl-oxygen is 1.784 Å with a total hydrogen bonding energy of 1.00 eV. Attempts to add a third hydrogen bond at the pyrrolidine nitrogen site fail, as the additional PVP molecule is repulsed from the ring. The C—N bond lengths in the pyrrolidine ring both decrease upon hydrogen bonding. Finally, we note that attempts to obtain a π-π complex between cotinine and 4VP indicate that the ring interactions are repulsive. Clearly, the DFT calculations indicate that cotinine will complex to the PVP host matrix with a greater binding energy than the nicotine template, forming a stiffer network, and the experimental results reflect the results of those calculations.

General discussion

The mechanical properties of the nicotine and cotinine templated PVP MIPs differ from the amino acid samples investigated earlier,[14] as in this study, the matrix with the reinserted template molecules has a greater hardness compared to the "as-produced" MIP polymer state. The hardness and the reduced modulus increase dramatically from 0.41 GPa and 11.1 GPa for the "as-produced" state, PVP-N, to 0.58 GPa and 18.9 GPa for the reloaded state, PVP-*N*-N. This represents a hardness and modulus increase of 41 and 70%, respectively. The same responses are observed for the PVP-C material system, although the effect on a percentage basis is less pronounced. Here, the hardness and the reduced modulus increase from 0.59 GPa and 14.7 GPa for the "as-produced" state, PVP-C, to 0.69 GPa and 15.7 GPa for the reloaded state, PVP-C-C. The hardness increases by 17% and the modulus by 7%. The DFT calculations predicted that the cotinine molecule would hydrogen bond more strongly with the polymer PVP matrix than the nicotine molecule. Therefore, the PVP-C MIP would be more stable than the PVP-N functional state. This is reflected experimentally in a larger hardness and reduced modulus for the PVP-C "as-produced" system. Reloading of the complementary molecule results in mechanical properties approaching those of the as-produced MIP of the reinserted material; insertion of the cotinine molecule into the PVP-N template removed MIP results in an increase of hardness and reduced modulus by 75 and 80%, respectively. Differing geometric parameters and bonding generate a strong increase of the mechanical parameters. On the other hand, the reloading of the nicotine molecule into the PVP-C template removed MIP system creates a softer material, as the hydrogen bonding of this molecule to the polymer is weaker than that of the original cotinine template; the PVP-C-N functional state presents a 19% lower hardness and a 14% lower modulus than the "as produced" PVP-C state. These values are similar to those of the "as-produced" PVP-N system. The trend is clear; for both systems, we have found that the reinsertion of the molecule for which the MIP has been templated makes the material stiffer than in the "as-produced" state, even though the extent of reinserted is 50% of the original film content. This behavior may be attributed to the fact that reintroduction of the template occurs primarily in the upper portion of the film and nanoindentation is sampling exactly this region. The increase in nanohardness with reinsertion of the analyte molecule is unique among the MIPs we have studied. In other studies, we have found that reinsertion of the analyte returns the nanomechanical properties to approximately, but slightly less than, those of the originally produced MIP.[14] The observation here, in a MIP that is considerably less porous than those for carbohydrates or amino acids, may be attributed to shrinkage of a film from which the template has been extracted during the aging process. PVP is known to provide gas-tight coatings in the case of polymer-coated foam shells.[32] In those same studies, the PVP coating was found to cause a densification of the foam core as the coating underwent shrinkage. If the bulk of the MIP film experienced the same shrinkage, in the extracted state, reinsertion of the template molecule (or the alternative analyte) would result in hydrogen bonding but not necessarily entirely within the molecular cavities. The hydrogen bond strengths would not necessarily differ, but the overall nanomechanical properties would be altered by these additional, nonspecific hydrogen bonds. As observed experimentally the control films exposed to the same treatment as the MIPs would not experience this effect, as the macropores and the molecular cavities were not present in the NIPs.

CONCLUSIONS

We have measured the nanomechanical properties of nicotine- and cotinine-imprinted poly(4-vinylphenol) films using depth sensing nanoindentation. These measurements have shown that:

- changes in the nanomechanical properties are correlated to the functional state of the imprinted polymer, allowing identification of the films in their "as produced" state, "template removed" state or "reloaded" state;

- the nanomechanical properties are capable of identifying which of the two template molecules, nicotine or cotinine, are inserted into a film when the templates are cross-introduced into emptied MIPs;
- the nanomechanical properties reflect the hydrogen bonding characteristics of the template molecules as determined through DFT calculations;
- reinsertion of a template molecule into a "template removed" film increases the nanohardness over the values recorded for the "as produced" film as a result of the physical properties of the polymer.

These results indicate that nanohardness measurements may be used as a reporting tool in the development of a new generation of sensors.

J. J. B. acknowledges the support of the Flight Attendants Medical Research Institute through the Richmond Center for Excellence of the American Academy of Pediatrics.

References

1. Marty, J. D.; Mauzac, M. Adv Polym Sci 2005, 172, 1.
2. Dufaud, V.; Bonneviot, L. In Nanomaterials and Nanochemistry; Brechignac, C., Houdy, P., Lahmani, M., Eds.; Springer: Berlin, 2008; p 597.
3. Kempe, H.; Kempe, M. In the Power of Functional Resins in Organic Synthesis; Tulia-Puche, J., Fibericio, F., Eds.; Wiley: Berlin, 2008.
4. Poma, A.; Turner, A. P. F.; Piletsky, S. A. Trends Biotechnol 2010, 28, 629.
5. BelBruno, J. J. Micro Nanosyst 2009, 1, 163.
6. Yanga, K.; Maa, J.; HZhoub, H.; Lia, B.; Yua, B.; Zhaoa, C. Desalination 2009, 245, 232.
7. Faizala, C. K. M.; Kikuchic, Y.; Kobayashi, T. J Membr Sci 2009, 334, 110.
8. Dima, S. O.; Sabru, A.; Dobre, T.; Bradu, C.; Antohe, N.; Radu, A.; Nicolescui, T.; Lungu, A. Mat Plastice 2009, 46, 372.
9. Chen, R. R; Qin, L.; Jia, M.; He, X. W.; Li, Y. J Membr Sci 2010, 363, 212.
10. Shneskoff, N.; Crabb, K.; BelBruno, J. J. J Appl Polym Sci 2002, 86, 3611.
11. Richter, A.; Gibson, U. J.; Nowicki, M.; BelBruno, J. J. J Appl Polym Sci 2006, 101, 2919.
12. Campbell, S. E.; Collins, M.; Lei, X.; BelBruno, J. J Surf Interface Anal 2009, 41, 347.
13. Sambe, H.; Hoshina, K.; Moaddel, R.; Wainer, I. W.; Haginaka, J. J Chromatogr A 2006, 1134, 88.
14. BelBruno, J. J.; Richter, A.; Campbell, S. E.; Gibson, U. J. Polymer 2007, 48, 1679.
15. Richter, A.; Gruner, M.; BelBruno, J. J.; Gibson, U. J.; Nowicki, M. Colloids Surf A 2006, 284/285, 401.
16. Fischer-Cripps, A. C. Nanoindentation; Springer: New York, 2002.
17. Olivier, W. C.; Pharr, G. M. J Mater Res 1992, 7, 1562.
18. Wolf, B.; Richter, A. New J Phys 2003, 5, 15.
19. IWard, I. M.; Hadley, D. W. An Introduction to the Mechanical Properties of Solid Polymers; John Wiley: Chichester, 1993.
20. Nowicki, M.; Richter, A.; Wolf, B.; Kaczmarek, H. Polymer 2003, 44, 6599.
21. Du, B.; Liu, J.; Zhang, Q.; He, T. Polymer 2000, 42, 5901.
22. Tsui, O. K.; Wang, X. P.; Ho, J. Y. L.; Nag, T. K.; Xiao, X. Macromolecules 2000, 33, 4198.
23. Richter, A.; Smith, R. Encyclopedia Nanosci Nanotechnol 2011, 17, 375.
24. Bronside, D. E.; Macosko, C. W.; Scriven, L. E. J Imaging Technol 1987, 13, 122.
25. Hysitron Inc. Hysitron User Handbook: Feedback Control Manual. Hysitron, Inc: Minneapolis, USA.
26. Richter, A.; Smith, R.; Dubrovinskaia, N.; Mcgee, E. High Pressure Res 2006, 26, 99.
27. Valiev, M.; Bylaska, E. J.; Govind, N.; Kowalski, K.; Straatsma, T. P.; van Dam, H. J. J.; Wang, D.; Nieplocha, J.; Apra, E.; Windus, T. L.; de Jong, W. A. Comput Phys Commun 2010, 181, 1477.
28. Adamo, C.; Barone, V. J Chem Phys 1998, 110, 6158.
29. Hariharan, P. C.; Pople, J. A. Theor Chim Acta 1973, 28, 213.
30. Avogadro, GNU Project. Available at: http://avogadro.openmolecules.net.
31. Breton, F.; Rouillon, R.; Pilestska, E. V.; Karim, K.; Guerreiro, A.; Chianella, I.; Piletsky, S. A. Biosens Bioelectron 2007, 22, 1948.
32. Nikroo, A.; Czechowicz, D.; Paguio, R.; Greenwood, A. L.; Takagi, M. Presented at the15th Target Fabricartion Specialists Meeting; Gleneden Beach, Oregon, June 1–5, 2003. General Atomics Report. Available at: https://fusion.gat.com/pubs-ext/TFSM03/A24451.pdf.

Research Article

Journal of Molecular Recognition

Received: 25 June 2013, Revised: 5 August 2013, Accepted: 30 September 2013, Published online in Wiley Online Library

(wileyonlinelibrary.com) DOI: 10.1002/jmr.2331

A selective molecularly imprinted polymer-carbon nanotube sensor for cotinine sensing

Sadik Antwi-Boampong[a], Kristina S. Mani[a], Jean Carlan[a] and Joseph J. BelBruno[a]*

Conductive composite films comprised of single-walled carbon nanotubes coated with molecularly imprinted poly-4-vinylphenol are produced and characterized using ultraviolet and infrared spectroscopies, confirming the successful molecular imprinting of the film with cotinine. The electrical resistance of the imprinted film changes significantly upon binding cotinine, by more than 30 kΩ, while the unimprinted film in comparison elicits little response. Additionally, once the cotinine template desorbs from the film, the resistance of the imprinted film returns to a value close to the pre-adsorption baseline. Scanning electron microscopy is used to study the morphology of the film compared with the unimprinted control, and gas chromatography quantitatively confirms that the imprinted film selectively detects cotinine while discriminating against the structurally similar alkaloid, nicotine. Copyright © 2013 John Wiley & Sons, Ltd.

Keywords: molecularly imprinted polymer; conductive sensor; cotinine; carbon nanotube composite; poly-4-vinylphenol; thin films

INTRODUCTION

Traditionally, the conceptualization, design, and fabrication of many chemical sensors have relied heavily on the integration of conductive polymers as an active layer, chief among them, polyaniline (Collins and Buckley, 1996; Janata and Josowicz, 2003; Virji, *et al*., 2004). In these sensors, the operating principle is based on changes in polymer conductivity following chemical detection of the analyte. Specifically, the conductive polymers interact with the target molecule through acid–base chemistry or a redox reaction, modulating the delocalization of π-electrons along the polymer backbone (Bai and Shi, 2007). The result is a change in the intrinsic conductivity of the polymer (Lange *et al*., 2008; Wan, 2008).

Despite the merits of conductive polymers for sensor development, there are also limitations. There are a number of important analytes with which conductive polymers lack the requisite chemical functionality to react, yielding only a tepid change in conductivity. Polyaniline is an illustrative example. Despite the widely reported sensing ability of polyaniline, the contiguous nitrogen centers that comprise its π-conjugated polymeric architecture have been found to be chemically unresponsive to a number of volatile organic compounds (Azim-Araghi and Jafar, 2010).

Lack of reactivity with key molecular species has sparked great interest in polyaniline functionalization and composite development (Hong *et al*., 2004; Wojkiewicz *et al*., 2011; Carquigny *et al*., 2012). Recent fabrication of chemical sensors has focused on developing molecularly imprinted polymer (MIP)-carbon nanotube (CNT) composite materials (Chen *et al*., 2010). This innovative engineering approach combines the enhanced chemical selectivity of an MIP with the extraordinary electrical properties of CNTs. Other researchers have coated the MIP directly onto the walls of functionalized CNTs, and here, we cite several of the more recent reports on this technology. Fluoroquinolones were extracted from eggs using a poly(methacrylic acid) MIP on magnetic CNTs, and the magnetic properties were used to isolate the polymers (Xiao *et al*., 2013). Chlorpyrifos have been separated from aqueous solutions using vinyl-functionalized CNTs (Anirudhan and Alexander, 2013), and a similar separation for ribavirin from solution was shown to be effective using a polyacrylamide MIP coated onto nanotubes (Xu and Xu, 2012). Finally, uric acid was detected by a PMAA coated CNT MIP (Chen *et al*., 2010). These are a few of the examples that demonstrate the utility of CNTs in sensing applications; however, none of these reports use the CNTs as the reporting agent for a sensing device.

Integration of the MIP-CNT composite in the sensing platform achieves two important goals. First, using an MIP maximizes the efficiency of the chemical detection of the target molecule because the imprinted polymer is, both chemically and structurally, imbued with an affinity for the target molecule (BelBruno, 2009; Haupt, 2010). Second, by coating the nanotubes with the imprinted polymer, the electrical properties of the nanotubes can be leveraged to enhance sensor conductivity, because the local conductivity of the nanotubes scales with analyte adsorption by the MIP.

Sensors fabricated from composite imprinted polymer/CNT materials provide the opportunity for great flexibility in polymer-host permutations, and they mitigate the functional strictures imposed by the use of conductive polymers. Recently, composite electrochemical sensors have been designed for biological (Cai *et al*., 2010), environmental (Huang *et al*., 2011), and especially pharmaceutical applications (Xing *et al*., 2012; Prasad *et al*., 2013). Though the detection systems reported in the literature typically

* *Correspondence to: J. BelBruno, Department of Chemistry, Dartmouth College, Hanover, NH 03755, USA.*
E-mail: jjbchem@dartmouth.edu

a *S. Antwi-Boampong, K. S. Mani, J. Carlan, J. J. BelBruno*
Department of Chemistry, Dartmouth College, Hanover, NH, 03755, USA

entail polymer functionalized single or multi wall CNTs, it is also possible to simply coat the nanotubes with the polymer in solution and cast the composite solution as a film across electrodes for chemical sensing (Manivannan *et al*., 2008). This technique is faster, simpler, less expensive, and can easily be scaled up.

In this study, we develop a sensitive poly-4-vinylphenol (PVP) imprinted—single wall nanotube (SWNT) sensor that selectively and rapidly detects cotinine, the principal metabolite of nicotine. The molecular structures of PVP, cotinine, and nicotine are shown in Figure 1. Cotinine is excreted from the body through urine (Paoletti *et al*., 1996). Selective detection and quantification of this biomarker in urine samples are thus an important diagnostic to monitor an individual's exposure to secondhand smoke. We have optimized the molecular detection of cotinine by harnessing the capacity of the PVP phenolic hydroxyl to hydrogen bond with the carbonyl moiety on cotinine. Additionally, the chemiresistor presented in this publication shows that molecular imprinting of PVP with cotinine yields polymeric scaffolds with cotinine-specific receptors that can discriminately bind cotinine.

We employ electrical conductivity measurements to show how the conductivity of our PVP-coated SWNT sensor is tempered by selective adsorption of cotinine. Ultraviolet (UV) and infrared (IR) spectroscopies are used to demonstrate the selective adsorption of cotinine by the imprinted PVP-coated SWNTs layer. Using gas chromatography (GC), we are able to quantitatively confirm cotinine imprinting of the composite layer and also establish the chemical preference of the sensor for cotinine over the structurally similar alkaloid, nicotine. Scanning electron microscopy is used to morphologically distinguish between the unimprinted and imprinted nanostructured composite films.

This work contributes to the fundamental knowledge on molecularly imprinted-CNT composite materials for electrochemical sensing; by demonstrating the efficacy of the imprinted-PVP/SWNT sensor for selective cotinine detection, it underscores the promise of this class of materials in detecting deleterious contaminants, pollutants, and other important biological molecules.

EXPERIMENTAL DETAILS

Materials

Poly-4-vinylphenol was purchased from Polysciences, Inc. with a molecular weight of 11,000. (−)-Cotinine (98%) and (S)-(−)-Nicotine (99%) were both obtained from Alfa Aesar. Methanol, the solvent used for preparing the composite casting solutions, was procured from Pharmco-Aaper. The single wall CNTs, which were 0.5–10 μm in length and 0.7–2.5 nm in diameter, were supplied by BuckyUSA. Toluene from Acros Organics was used for preparing cotinine solutions as well as for the removal of the cotinine template from the imprinted films. All reagents and materials are used as received without any further treatment.

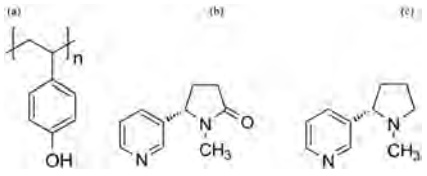

Figure 1. Molecular structures of (a) poly(4-vinylphenol) (b) cotinine, and (c) nicotine.

Preparation of molecularly imprinted polymer-single wall nanotube casting solutions

The experimental protocol, beginning with interdigitated electrode (IDE) production and proceeding through to sample measurement is shown in Figure 2. A 10% w/v PVP-1% SWNT solution is prepared by dissolving 1 g of PVP and 0.1 g of SWNTs in 10 ml of methanol. This solution serves as the control (unimprinted) composite solution. To make the MIP casting solution, 1 g of PVP, 0.1 g of SWNTs, and 0.5 g of cotinine are dissolved in 10 ml of methanol. All of the solutions are then stirred with a magnetic stirrer overnight. The coating of the SWNTs by the imprinted and unimprinted PVP is evident by the complete suspension of the nanotubes in the methanol solution. The bare nanotubes are hydrophobic and therefore do not suspend in a polar solvent like methanol. However, when the nanotubes are mixed with the PVP, the polymer chains become tethered to the nanotubes, and the interfacial adhesion between polymer and nanotube yields a hydrophilic material that remains permanently suspended in methanol.

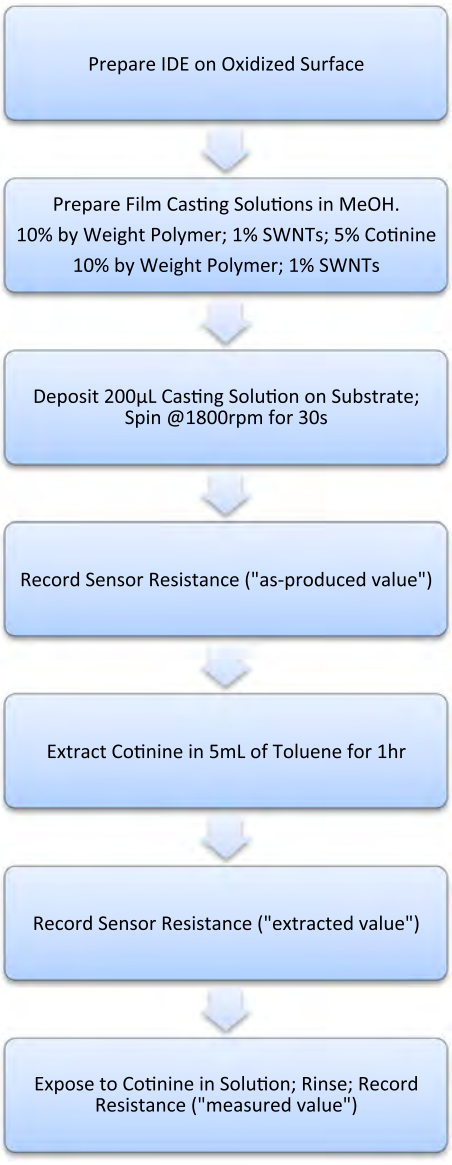

Figure 2. Flow diagram for the preparation of imprinted and control sensors.

Journal of Molecular Recognition

Fabrication of sensor and conductivity measurement

Silicon substrates thermally oxidized with a 5000 Å oxide layer are used to construct the conductive sensors with the MIP-coated nanotubes as the active layer that bridges the gap between the electrodes. The oxide layer isolates the network of IDEs from the silicon surface and prevents the sensor from shorting. Chromium was selected to make the interdigitated microelectrode grid because it adheres well to the silicon surface and has a high conductivity suitable for our studies. To produce the IDEs, a 1000 Å layer of chromium is deposited onto the silicon, patterned by conventional photolithography and wet etched to produce the IDE array that occupies a total area of 376 mm^2. The final lift off process is performed using acetone and ample amounts of water. The final product, the interdigitated microelectrode grid shown in Figure 3, comprises 40 μm fingers with 20 μm spacing. Not chosen arbitrarily, the finger dimensions and spacing used for the sensor fabrication are based on previous work performed in our research group (Antwi-Boampong and BelBruno, 2013) that showed that such an IDE configuration eliminates production defects and optimizes sensor response.

After fabrication, the sensors are cleaned with acetone before measurements. A 200-μl aliquot of solution is pipetted onto the electrodes, and the spin coater is accelerated at 1800 rpm for 30 s to produce a film with a thickness of about 300 nm. The spin coating parameters used are based on previous experiments, and the thin films produced via this spin coating technique are characteristically consistent in thickness and uniformity. After casting the films on the electrodes, the resistance of the films is measured. The conductive film bridges the gap between the IDEs, thereby completing the circuit. Resistance readings are therefore solely the resistance of the spin-cast film. A Keithley Model 2100 6 ½ Digit Multimeter (Keithley Instruments, Inc., Cleveland, OH 44139, USA) is used to measure the resistance of the composite polymer films. During resistance measurements, the meter supplies a 1 mA current through the film, and from the resulting voltage, the film resistance is algorithmically calculated using Ohm's law. The films do not heat up because the power dissipated through them during measurements is less than 500 mW. All reported data are measured using two contacts instead of four point measurements because the two-contact method is simple, straightforward, and suitable for this investigation. Additionally, the simpler DC measurement is used because there is no significant noise interference during the measurements.

The resistance of the MIP-SWNT film is measured directly after casting, and the reading is recorded as the "as-produced" value. Next, the cotinine molecule is extracted from the sensor layer by placing the sensor in 5 ml of toluene for an hour. Toluene preferentially extracts cotinine from the matrix without chemically affecting the PVP. Following cotinine removal from the MIP film, the sensor is dried with a jet of nitrogen gas, and the resistance of the sensor is measured again to obtain the "extracted" value for the MIP. In the final step, the MIP extracted sensor is exposed to cotinine by placing it in a 5% cotinine in toluene solution for up to 1 hour. This controlled exposure facilitates the reinsertion of the template into the cotinine-specific cavities imprinted in the MIP film. After reinsertion, the sensor is rinsed with toluene to remove any excess cotinine that could adhere to the sensor. Then, the sensor is dried with nitrogen gas, and the resistance of the sample is measured again to yield the value for the cotinine "reinserted" or measured results for the MIP. The same protocol for the conductivity measurements detailed previously is repeated for the unimprinted PVP-coated SWNT (control sensor). The results for the imprinted and unimprinted sensors are then compared. Selectivity of the imprinted sensor for cotinine is studied by exposing the sensor to a 5% nicotine solution.

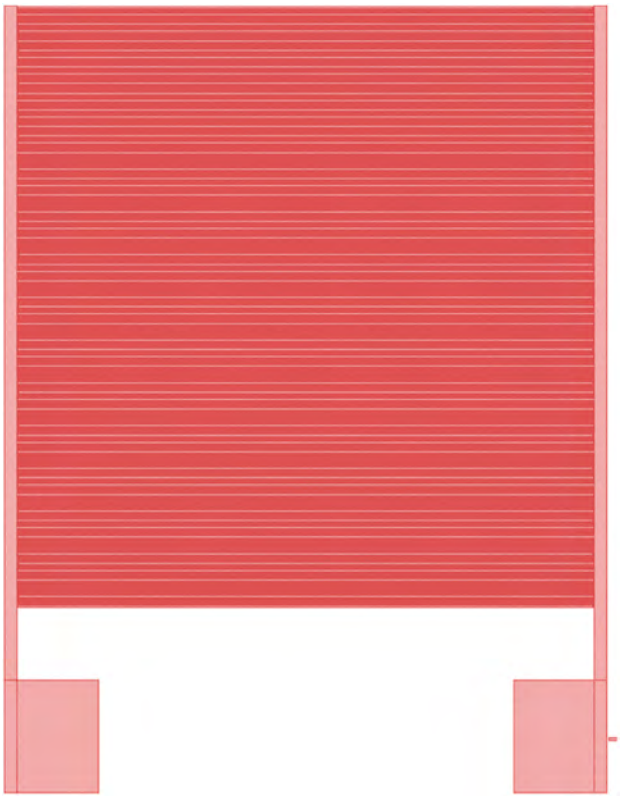

Figure 3. Schematic depiction of the lithographically patterned interdigitated electrode array: fingers are 40 μm with a 20-μm spacing.

Spectral characterization of molecularly imprinted polymer-single wall nanotube coated film

Using UV spectroscopy, the successful cotinine imprinting of the imprinted PVP-coated nanotube is confirmed. The imprinted and unimprinted sensors are submerged in two separate 5 ml water vials for an hour, and 1 ml of each solution is used for UV analysis to generate the UV spectra for the control and the imprinted sensors.

A more extensive chemical characterization of the control and imprinted sensors is performed using IR spectroscopy. Here, the composite films are spin cast onto 1-inch square glass slides that are well-suited for spectroscopic studies of thin films. IR spectroscopy is utilized to qualitatively confirm the imprinting of the film with cotinine. The attenuated total reflection IR spectrum of the MIP layer is measured directly after casting the MIP layer. The film is then extracted in 5 ml of toluene for an hour to remove the cotinine template from the film, and the IR spectrum is recorded. Next, the same film is placed in 5 ml of a 5% cotinine in toluene solution to reinsert the template into the film, and the IR spectrum for the reinserted film is measured. The same procedure is applied to the control films, and the IR spectra are measured at each stage—after casting, extraction, and reinsertion. The spectra for the imprinted and unimprinted layers at the various stages are compared and contrasted.

Gas chromatography measurements

Gas chromatography (GC) measurements are performed to quantitatively confirm the imprinting of PVP with cotinine. For cotinine GC analysis, a Perkin Elmer AutoSystem XL gas chromatograph with a flame ionization detector (Perkin-Elmer Corp., Waltham, MA 02451, USA) is used, and the GC column is a Supelco Equity 5 column (30 m, 0.25 μm film thickness, 0.25-mm i.d.). The carrier gas, helium, is set to a head pressure of 15 psi., and the temperature program is 90°C (held for 2 min), ramping 15°C/min to 180°C (held for 2 min) and then a final ramp of 40°C/min to 280°C (held for 4 min). The flame ionization detector temperature is programmed to 300°C. The standard split/splitless liner is used in the injection port that is set to 280°C. Sample volumes of 1.6 μl are injected with a split ratio of 30:1. Calibration standards ranging from 17 to 250 μg/ml cotinine in toluene along with an internal standard, quinoline, are used to create a calibration curve with a typical $R^2 = 0.997$. The instrument is checked daily for calibration using a midpoint calibration standard. Recalibration is required if the result deviates more than 10% from actual cotinine concentration. In addition, the quality of peak shapes, resolution, and retention times were carefully monitored to ensure that all chromatographies were within acceptable ranges. The average standard deviation for the chromatography results reported is 16%.

The amount of cotinine present in the MIP-coated SWNT sensor is determined by immersing the sensor in toluene solution to fully extract the cotinine, and an aliquot of the supernatant liquid is GC analyzed. The as-produced unimprinted sensor is also treated in a similar fashion and is analyzed. Results from this analysis are indicative of the amount of cotinine imprinted in the composite MIP sensor. To probe the sensitivity of the MIP-coated SWNT to cotinine molecules, the control and MIP sensors concomitantly undergo the extraction procedure in toluene and are reinserted in cotinine solutions as described in the Fabrication of Sensor and Conductivity Measurement section. Once cotinine reinsertion is completed, the sensors are soaked in a toluene extraction solution to remove all bound cotinine molecules from the composite films. Volumetrically equivalent aliquots from the supernatant solution are then subsequently analyzed via GC to determine how much cotinine is detected by both control and imprinted sensors during the reinsertion procedure.

Finally, to establish the selectivity of the MIP-SWNT sensor, the extracted MIP-coated SWNT sensor is exposed to nicotine molecules via immersion in a 5% nicotine toluene solution. The behavior of the sensor during this sustained exposure to nicotine is a litmus test of sensor selectivity. Given that nicotine is a chemically and structurally similar alkaloid, it is the best candidate to elucidate the sensor selectivity.

Morphological Studies of the molecularly imprinted polymer-single wall nanotube films

An FEI Co. XL-30 ESEM-FEG field emission gun, environmental scanning electron microscope (FEI Company, Hillsboro, OR 97124, USA) is employed to probe the composition and microstructure of the imprinted and unimprinted composite films. All films are imaged at equivalent length scales using the secondary electron mode.

RESULTS AND DISCUSSION

The distinct change in the electrical resistance of the polymer-coated SWNT layer of the sensor device is the physical property measured to determine the immediate detection of cotinine. Cotinine adsorption by the active layer alters the conductivity —and inversely, the resistance—of the sensor, and this resistance variation is analyzed. Conductivity measurements are the central focus of this work, and the values collated for the imprinted and unimprinted sensors are compared. On average, the resistance of the as produced, imprinted sensor containing cotinine is about 36 kΩ greater than the unimprinted sensor. Extracting the imprinted sensor yields an average resistance of 6.6 kΩ, and following reinsertion, the average resistance of the sensor becomes 43.6 kΩ. For example, for a characteristic run, the absolute resistance of the unimprinted sensor is 4.58 kΩ. In sharp contrast, the imprinted sensor has a significantly greater resistance of 47.87 kΩ—a value that exceeds the control sensor's resistance by more than 900%. When the cotinine template is extracted from the imprinted sensor in toluene, its resistance drops sharply to 6.56 kΩ. It is worth noting that the removal of the cotinine template from the imprinted sensor essentially yields an absolute resistance that is barely at variance with the control sensor. Following reinsertion of cotinine into the imprinted film, the sensor resistance immediately increases from 6.56 to 46.19 kΩ, a value similar to the resistance of the as-produced MIP sensor. Conversely (and expectedly), the resistance of the as-produced unimprinted sensor barely changes after going through the extraction and cotinine reinsertion procedures. In fact, when exposed to cotinine, the sensor resistance increased by only 75 Ω. This diametric resistive response of the unimprinted and control layers is in agreement with the transduction mechanism hypothesized. After exposing the imprinted sensor to 5% nicotine, the resistance increases slightly from 6.72 to 8.11 kΩ—an insignificant change compared with the sensor response to an equivalent amount of cotinine.

Most of the previous literature involving MIP-coated CNTs utilized multiwalled CNTs (MWNTs), but those studies used the CNTs as a support rather than a reporting agent. MWNTs are commonly metallic in nature. The conducting property of metallic nanotubes renders them less sensitive when applied as sensors. SWNTs have been demonstrated to have larger changes in conductivity, up to three orders of magnitude as compared with MWNTs, when deployed as sensors (Bandaru, 2007), hence their application to the problem at hand. SWNT-polymer sensor devices are acutely sensitive to adsorption of molecules because any change in the local chemical environment of the coated nanotubes triggers an appreciable energy level perturbation in the CNT conduction channel. This electronic tumult—however subtle—manifests as a detectable change in conductance and is the output measured to confirm binding of the analyte. Nanotubes are intrinsically *p*-type structures, that is, the majority carriers are holes (Bandaru, 2007). If the nanotubes are brought into contact with a reducing agent, charge is transferred to the nanotubes, and the conductance (due to the holes) is decreased. The MIP-coated PVP nanotube sensor we have developed functions in this manner, as a *p*-type semiconducting sensor device, where the detection of the cotinine molecule with its abundance of π-electrons educes a significant resistance increase. We postulate the transduction mechanism of our sensor based on a molecular understanding of the chemical interaction between the composite polymer layer and the cotinine template. The PVP-coated MIP layer binds the carbonyl on the cotinine lactam group as well as the nitrogen of the pyridine ring with the hydroxyl group of the polymer to form hydrogen bonds. The proximity of cotinine and the ensuing chemical interaction with the polymer both

disrupt the nanotube electronic structure and leads to an influx of electron density in the CNT conduction pathway that reduces the CNT charge mobility (Martel *et al*., 1998; Roman *et al*., 2004; Kauffman and Star, 2008).

Ultraviolet and IR spectroscopy studies qualitatively confirm imprinting, show the nature of the chemical interactions, and demonstrate the selectivity of the MIP sensor for cotinine. UV characterization of the control sensor yields a flat spectrum, while the spectrum for the MIP sensor has the prominent cotinine peak at 262 nm.

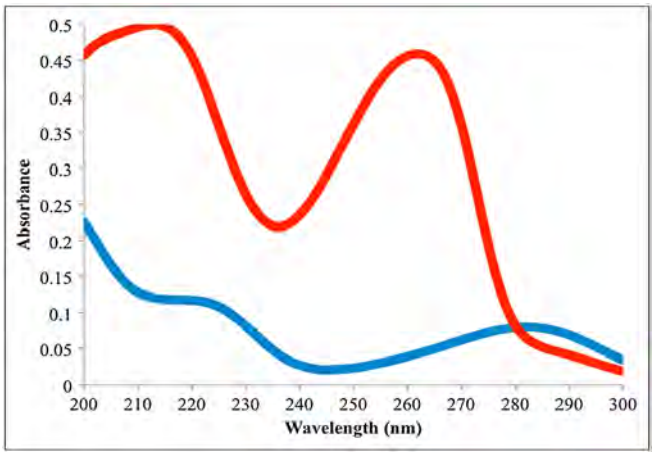

Figure 4. Ultraviolet spectra for control composite film (blue) and molecularly imprinted polymer-coated nanotube composite film (red).

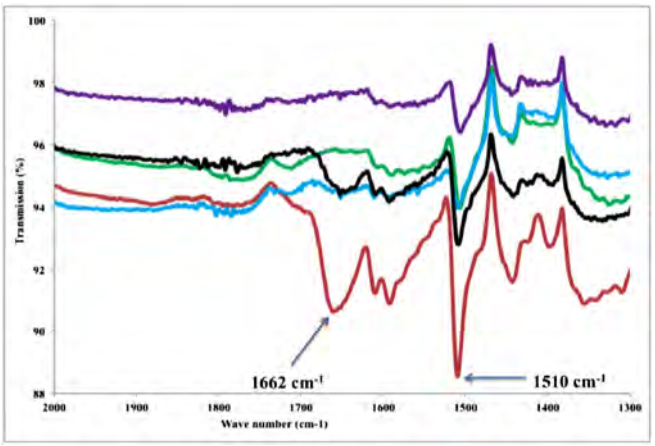

Figure 5. Infrared spectra of control (green), molecularly imprinted polymer (MIP) (red), MIP extracted (blue), MIP reinserted (Black), and control reinserted (purple).

Figure 4 is the juxtaposed UV spectra of the as-produced control (blue) and MIP (red) layers. The cotinine peak found only in the MIP spectrum at a notably high absorbance (0.4) indicates that the film is effectively imprinted with cotinine.

Detailed spectroscopic study of the sensor layers is achieved by IR spectroscopy. IR spectra for the control, MIP, MIP extracted, MIP reinserted, and control reinserted samples are generated. Figure 5 is a juxtaposition of all of the spectra. There is a sharp absorption band at 1662 cm^{-1} in the MIP spectrum belonging to the cotinine C = O vibration stretching that is absent in the control. Equally important, the occurrence of the cotinine carbonyl adsorption band in the MIP film at 1662 cm^{-1} instead of the 1690 cm^{-1} peak (Borden *et al*., 2003) that occurs in neat cotinine indicates that the cotinine molecule is hydrogen bonded to the hydroxyl group in the imprinted polymer. Additional evidence of cotinine bonding in the MIP film is the presence of the strong carbon—carbon bands at 1510 cm^{-1}. Extraction of the cotinine template with toluene results in the disappearance of the cotinine carbonyl band from the MIP spectrum, while the IR spectrum of the reinserted MIP sensor film in the cotinine solution shows the reappearance of the carbonyl peak. In contrast, the IR spectra taken for the control after extraction and reinsertion show no cotinine peaks similar to the bands identified in the MIP and reinserted MIP spectra. The absence of the carbonyl peak in the reinserted control film is evidence that the MIP-coated SWNT layer selectively adsorbs the cotinine molecules.

These analytical data provide information on the ability of the MIP to recognize the template. While the exact mechanism of recognition cannot be stated with absolute certainty, we speculate, based on previous imprinting experience and the peaks in the IR and UV spectra of cotinine in isolated and imprinted situations, that both hydrogen bonding and shape recognition occurred. The carbonyl oxygen and pyridyl nitrogen on the cotinine interacted with the phenolic hydrogen in the polymer to add a chemical component to the shape-recognition sites in the MIP. It is this chemical component to the recognition that allows discrimination of cotinine from nicotine. The template molecule is a nucleophile, that is, it is relatively electron rich. The imprinted polymer contains this electron-rich template that, at the imprint sites, has the ability to add charge to the electrical environment, increasing the resistance of the semiconducting CNTs.

Gas chromatography data mirror the results obtained for the conductivity and spectroscopic measurements. A typical chromatogram from our cotinine analysis is shown in Figure 6. In addition to

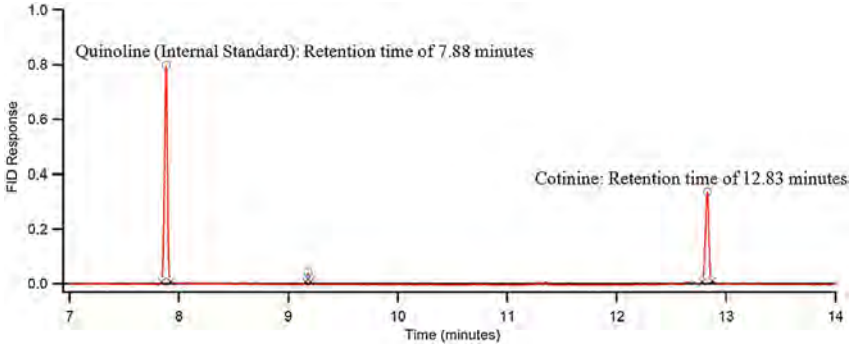

Figure 6. Typical gas chromatographic analysis of cotinine extracted from the sensors.

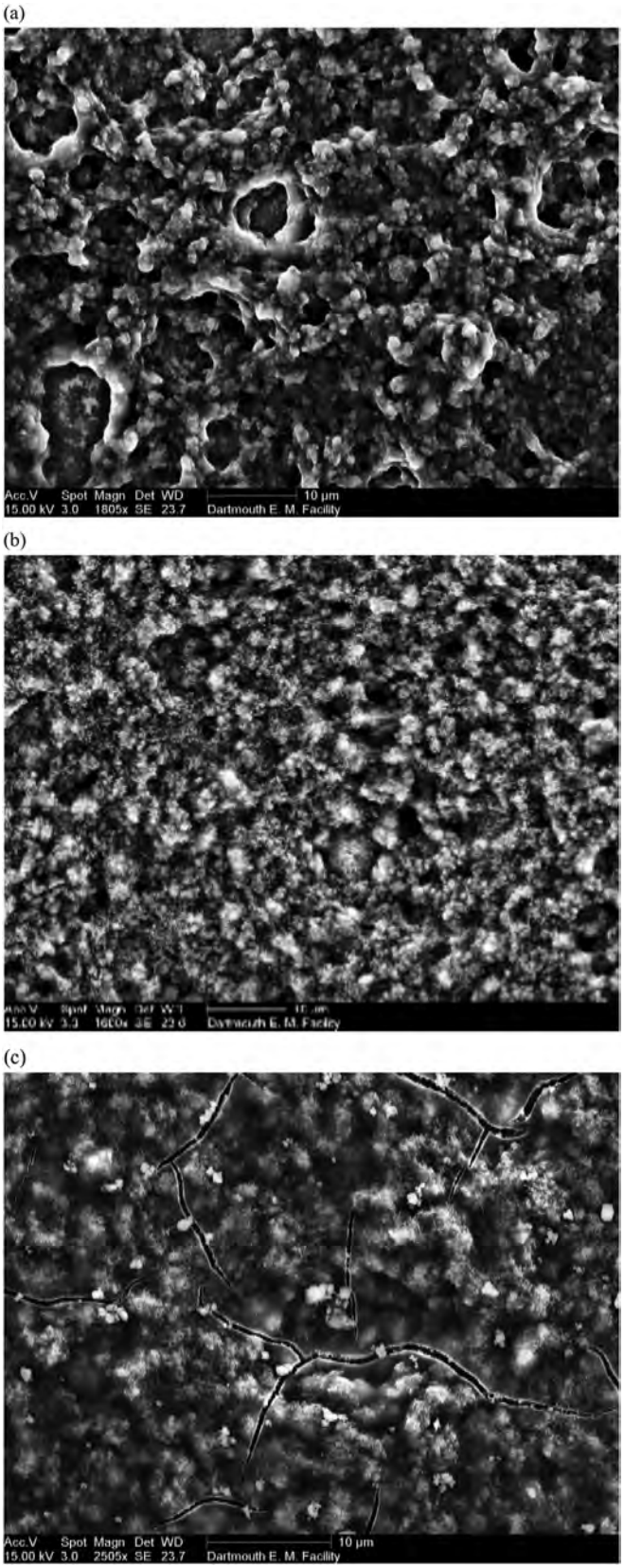

Figure 7. Scanning electron microscope micrographs of control (a), molecularly imprinted polymer containing template (b), and molecularly imprinted polymer extracted (c). All scanning electron microscope images have the same scales and are processed using the same parameters with IMAGE J software (Rashand, 2012).

confirming the effectiveness of the sensor, the GC results also show the ability of the sensor to distinguish between cotinine and nicotine molecules. The GC measurements reveal that the imprinted PVP-coated SWNTs adsorb 236 μg of cotinine, while the control unimprinted layer binds only 78 μg of cotinine—a difference of more than 200%. When the MIP sensor is applied to nicotine, it barely detects the nicotine molecules. In fact, while the MIP sensor detects 236 μg of cotinine, it only binds 16 μg of nicotine. Even more compelling, when the sensor is applied in a binary solution containing equal amounts of cotinine and nicotine, the sensor detects 1033% more cotinine than nicotine. Therefore, using GC, we were able to establish the sensor sensitivity as well as selectivity for cotinine detection. It is worth noting that the cotinine-specific cavities present in the imprinted film are structurally configured to detect cotinine, and as a result of the shape and chemical recognition processes, these cavities are able to exclude nicotine, which is smaller than the cotinine molecule and, lacking the carbonyl group, would not bind as strongly as the cotinine molecule.

The morphologies of the control, cotinine imprinted, and cotinine extracted nanotube films shown in Figure 7 are porous with the CNTs well dispersed in the polymer matrix. In addition to being porous, the cotinine imprinted film is relatively spongier than the other films, while the extracted MIP film is contoured by a network of cracks. Given that the MIP extracted imprinted film adsorbs significantly more cotinine than the unimprinted film, the presence of the deep fissures propagating through the MIP extracted layer indicates that imprinting the film incorporates nanoscale physico-structural features that facilitate the recognition and uptake of the analyte. Therefore, the cracks are active transport channels that minimize diffusional constraints and enhance template binding by the sensor layer.

On the basis of the electrical response of the sensor and the chromatographic analysis, the sensor's detection limit was calculated to be at least 0.05 ppm of cotinine. While this detection limit was used to demonstrate the potency of the sensor, we contend that it is within the realm of possibility for the sensor to detect significantly lower concentrations of cotinine by optimizing the active layer's properties like film thickness and porosity. This can be achieved by appropriately modifying the spin casting parameters. To ensure reproducibility, the electrical measurements were performed in triplicate during experimentation, and each experiment was performed with a newly fabricated sensor. The average standard deviation for the sensor's molecular recognition of the cotinine template was 2.1%, and the sensor could be used serially for sensing activity after extracting the template. Due to the polymeric nature of the active layer, the sensor has a robust quality that makes it impervious to degradation by harsh agents or conditions. In addition to its excellent stability, the sensor layer can easily be regenerated for multiple usage thereby making it a suitable tool for assaying different samples without compromising its effectiveness. After production, the sensor's signal was measured within a time frame of a week—a strong indicator of the device's longevity.

CONCLUSION

In this work, we develop a viable imprinted polymer-based sensor that exhibits notable sensitivity and selectivity for cotinine detection. The sensor is a conductive polymeric composite film comprised of single wall CNTs coated with a cotinine imprinted PVP layer. In order

Journal of Molecular Recognition

to quantify the response of the imprinted film, we also synthesize a control lacking the cotinine imprint.

The imprinted and control films are characterized by electrical conductivity, GC, and IR spectroscopy. We show that adsorption of the template molecule cotinine results in a chemical change in the sensor. In particular, cotinine adsorption generates a resistance change of more than 30 kΩ (900% greater than the control), and remarkably, the chromatographic results show that the imprinted layer adsorbs 200% more cotinine than the unimprinted film. We attribute the sensitivity and selectivity of the sensor to the imprinting of the cotinine molecule, which imbues the sensor with the ability to discriminately detect cotinine.

The class of molecularly imprinted-CNT nanomaterials studied here is part of a paradigm shift in the design of high-performing electrochemical sensors, as they do not rely on conductive polymers to perform their function. The use of imprinted polyvinyl-4-phenol-coated SWNTs as a sensing layer in selectively detecting cotinine shows that this class of composite materials holds great promise in the development of molecular sensors that can specifically encode and bind a wide array of molecules. We measure reproducible changes in nanotube resistance induced by the chemical interaction between polymer and analyte. The significant (selective) response of the sensor to the analyte demonstrates that CNTs are a valuable component that can be coupled with polymeric materials for sensor fabrication.

Acknowledgements

We are grateful to the Richmond Center of Excellence of the American Academy of Pediatrics, the Flight Attendants Medical Research Institute, and the Women in Science Program at Dartmouth College for their financial support.

REFERENCES

Anirudhan T, Alexander S. 2013. Synthesis and characterization of vinyl-functionalized multiwalled carbon nanotubes based molecularly imprinted polymer for the separation of chlorpyrifos from aqueous solutions. *J. Chem. Technol. Biotechnol.* **88**: 1847–1858.

Antwi-Boampong S, BelBruno, JJ. 2013. Detection of formaldehyde vapor using conductive polymer films. *Sens. Act. B* **182**: 300–306.

Azim-Araghi ME, Jafar MJ. 2010. Electrical and gas sensing properties of polyaniline-chloroaluminium phthalocyanine composite thin films. *Eur. Phys. J. Appl. Phys.* **52**: 10402–10407.

Bai H, Shi G. 2007. Gas sensors based on conducting polymers. *Sensors* **7**: 267–307.

Bandaru PR. 2007. Electrical properties and applications of carbon nanotube structures. *J. Nanosci. Nanotech.* **7**: 1–29.

BelBruno JJ. 2009. Molecularly imprinted polymers: artificial receptors with wide-ranging applications. *Micro Nanosystems* **1**: 163–180.

Borden JT, Man A, Scott DA, Liu KZ. 2003. Tobacco-induced alterations to the Fourier-transform infrared spectrum of serum. *J. Mol. Med.* **81**: 788–794.

Cai D, Ren L, Zhao H, Xu C, Zhang L, Yu Y, Wang H, Lan Y, Roberts MF, Chuang JH, Naughton MJ, Ren Z, Chiles TC. 2010. A molecular-imprint nanosensor for ultrasensitive detection of proteins. *Nat. Nanotechnol.* **5**: 597–601.

Carquigny S, Redon N, Plaisance H, Reynaud S. 2012. Development of a polyaniline/fluoral-P chemical sensor for gaseous formaldehyde detection. *IEEE Sens. J.* **12**: 1300–1306.

Chen P-Y, Nien P-C, Hu C-W, Ho K-C. 2010. Detection of uric acid based on multi-walled carbon nanotubes polymerized with a layer of molecularly imprinted PMAA. *Sens. Act. B* **146**: 466–471.

Collins GE, Buckley LJ. 1996. Conductive polymer-coated fabrics for chemical sensing. *Syn. Met.* **78**: 93–101.

Haupt K. 2010. Biomaterials: Plastic antibodies. *Nat. Mat.* **9**: 612–614.

Hong K, Oh KW, Kang TJ. 2004. Polyaniline–nylon 6 composite fabric for ammonia gas sensor. *J. Appl. Polym. Sci.* **92**: 37–42.

Huang J, Xing X, Zhang X, He X, Lin Q, Lian W, Zhu H. 2011. A molecularly imprinted electrochemical sensor based on multiwalled carbon nanotube-gold nanoparticle composites and chitosan for the detection of tyramine. *Food Res. Int.* **44**: 276–281.

Janata J, Josowicz M. 2003. Conductive polymers in electronic chemical sensors. *Nature Mat.* **2**: 19–24.

Kauffman D, Star A. 2008. Carbon nanotube gas and vapor sensors. *Angew. Chem. Int. Ed.* **47**: 6550–6570.

Lange U, Roznyatovskaya N, Mirsky V. 2008. Conducting polymers in chemical sensors and arrays. *Anal. Chim. Acta* **614**: 1–26.

Manivannan S, Jeong IO, Ryu JH, Lee CS, Jang J, Park KC, Kim KS. 2008. Dispersion of single-walled carbon nanotubes in aqueous and organic solvents through a polymer wrapping functionalization. *J. Mater Sci-Mater Electron.* **20**: 223–229.

Martel R, Schmidt T, Shea HR, Hertel T, Avouris P. 1998. Single and multi-wall carbon nanotube field-effect transistors. *Appl. Phys. Lett.* **73**: 2447–2449.

Paoletti P, Fornai E, Maggiorelli F, Puntoni R, Viegi G, Carrozzi L, Corlando A, Gustavsson G, Sawe U, Giuntini C. 1996. Importance of baseline cotinine plasma values in smoking cessation: results from a double-blind study with nicotine patch. *Eur. Respir. J.* **9**: 643–651.

Prasad BB, Prasad A, Tiwari MP. 2013. Multiwalled carbon nanotubes-ceramic electrode modified with substrate selective imprinted polymer for ultra-trace detection of bovine serum albumin. *Biosen, Bioelect.* **39**: 236–243.

Rashand WS, 1997–2012. US National Institutes of Health. Bethesda, MD, USA. http://imagej.nih.gov/ij/

Roman C, Ciontu F, Courtois B. 2004. Aromatic amino acids physisorbed on graphene: electronic properties and Hamiltonian model reduction. *European Micro and Nano Systems.* **263**: 273–278.

Virji S, Huang J, Kaner R, Weiller B. 2004. Polyaniline nanofiber gas sensors: examination of response mechanisms. *Nano Lett.* **4**: 491–496.

Wan M. 2008. Conducting polymers with micro or nanometer structure. Springer.

Wojkiewicz L, Bliznyukc VN, Carquigny S, Elkamchia N, Redona N, Lasri T, Pude AA, Reynaud S. 2011. Nanostructured polyaniline-based composites for ppb range ammonia sensing. *Sens. Act. B* **160**: 1394–1403.

Xiao D, Dramou P, Xiong N, He H, Yuan D, Dai H, Li H, He X, Peng J, Li N. 2013. Preparation of molecularly imprinted polymers on the surface of magnetic carbon nanotubes with a pseudo template for rapid simultaneously extraction of four fluoroquinolones in egg samples. *Analyst* **138**: 3287–3296.

Xing X, Liu S, Yu J, Lian W, Huang J. 2012. Electrochemical sensor based on molecularly imprinted film at polypyrrole-sulfonated graphene/hyaluronic acid-multiwalled carbon nanotubes modified electrode for determination of tryptamine. *Biosen. Bioelect.* **3**: 277–283.

Xu L, Xu Z. 2012. Molecularly imprinted polymer based on multiwalled carbon nanotubes for ribavirin recognition. *J. Polym. Res.* **19**: 9942–9947.

